

Technical Report CHL-98-xx  
August 1998

# **CGWAVE: A Coastal Surface Water Wave Model of the Mild Slope Equation**

by

Zeki Demirbilek  
U.S. Army Corps of Engineers  
Waterways Experiment Station  
3909 Halls Ferry Road  
Vicksburg, MS 39180-6199

Vijay Panchang  
University of Maine  
School of Marine Sciences  
Libby Hall  
Orono, ME 04469-5706

Approved for Public Release; Distribution Is Unlimited

Prepared for Headquarters, U.S. Army Corps of Engineers

# CONTENTS

PREFACE .....	viii
CONVERSION FACTORS, NON-SI TO SI UNITS OF MEASUREMENT .....	ix
1. INTRODUCTION .....	1
2. BASIC EQUATIONS .....	6
3. BOUNDARY CONDITIONS .....	9
4. FINITE ELEMENT FORMULATION .....	12
4.1 Open Sea Problems .....	12
4.2 Harbor Problems .....	26
4.3 Alternative Open Boundary Treatment .....	27
4.4 Kinematic Parameters .....	37
4.5 Floating Docks .....	40
5. ITERATIVE CG SOLUTION METHOD .....	42
6. GENERATION OF FINITE-ELEMENT NETWORK .....	45
7. PROCEDURE FOR STAND-ALONE USAGE OF CGWAVE .....	46
7.1 File Descriptions .....	47
7.2 Raw Data Processing – Program “resol” .....	48
7.2.1 Viewing XYZ Data and Selecting Open Boundary End Points .....	49
7.2.2 XYZ File Format .....	50
7.2.3 Program “resol” .....	51
7.3 Creation of Finite Element Grid .....	53
7.3.1 Geometry .....	54
7.3.2 Boundary Conditions .....	55
7.4 The General Information File (*.gen) .....	57
7.5 Assembly of Input Information - Program “reform” .....	59
7.6 The Wave Model - Program “cgwave” .....	61
7.7 Post-processing the Output - Program “trans” .....	61
7.7.1 Program “trans” .....	62
7.7.2 Selected Output at Points/Lines/Rectangular Sub-regions. ....	63
7.8 Viewing Solutions in SMS .....	66
7.9 Instructions for CGWAVE Interface in SMS (MODE-2 Usage) .....	68
7.9.1 Creating a Size Function .....	68
7.9.2 Creating the Background Scatter Set .....	69
7.9.3 Creating the Coastline and Inlet Arcs .....	69
7.9.4 Defining Domains .....	70
7.9.5 Assigning Reflection Coefficients .....	71
7.9.6 Assigning Open Ocean Attributes .....	71
7.9.7 Setting the Active Scatter Data Function .....	71
7.9.8 Creating a Mesh from Feature Objects .....	72
7.9.9 Saving the CGWAVE .dat and .xyz (1-d) Files .....	72
7.9.10 Checking Mesh Quality .....	72

7.9.11 Running CGWAVE.....	73
8. EXAMPLES .....	74
8.1 Shoal on a Sloping Beach.....	74
8.2 Irregular Wave Propagation Over a Shoal .....	80
8.3 Rectangular Harbor - Resonance .....	91
8.4 Circular Island.....	97
8.5 Ponce de Leon Inlet, FL.....	99
8.6 Barbers Point Harbor, HI.....	103
8.7 Onslow Bay, NC.....	106
References .....	109

SF298

# LIST OF FIGURES

Figure 1. Definition Sketch of Model Domain.....	11
Figure 2. Definition Sketch.....	13
Figure 3. A Typical Element.....	14
Figure 4. Boundary Segments.....	19
Figure 5. Definition Sketch for Line Integrals Along the Open Boundary $\Gamma$ .....	23
Figure 6. Definition Sketch for Floating Structures.....	41
Figure 7. Modeled Domain of Berkhoff et al. (1982). ....	76
Figure 8. Wave Height Comparisons for a Low Resolution Domain.....	77
Figure 9. Wave Height Comparisons for Increasing Domain Resolutions. ....	78
Figure 10. Wave Height Comparisons from Linear and Non-linear CGWAVE Runs on a Domain Resolution of 15 Points per Wavelength. ....	79
Figure 11. Model Domain for Wave Propagation over an Elliptic Shoal [after Vincent and Briggs (1989)]. ....	85
Figure 12. Domain without Coastal Boundary Effects.....	85
Figure 13. Wave Height Comparisons for M1 Input Condition.....	86
Figure 14. Wave Height Comparisons for M2 Input Condition.....	87
Figure 15. Estimated Wave Heights for B1 Input Spectrum, 20° Directional Discretization. ....	88
Figure 16. Wave Height Comparisons for B1 Input Condition, 4.14° Directional Discretization. ....	89
Figure 17. Wave Height Comparisons for N1 Input Condition, 4.14° Directional Discretization. ....	90
Figure 18. Rectangular Resonance Harbor with Semi-circular Open Boundary.....	93
Figure 19. Theoretical and Numerical Resonance Curves for a Fully Reflecting Rectangular Harbor. ....	94
Figure 20. Harbor Response Curves for Various Values of Coastal Reflection Coefficient. ....	95
Figure 21. Harbor Response Curves for Various Values of Friction Factor. ....	96
Figure 22. Cross Section of Island and Shoal Bathymetry. ....	98
Figure 23. Comparison of Analytic and Numerical Wave Amplitudes.....	98
Figure 24. Phase Diagram for Normal Incident Direction, 15-second Period Wave Condition. ....	100
Figure 25. Estimated Wave Height Diagram for Normal Incident Direction, 15-second Period Wave Condition.....	101
Figure 26. Comparison Between Laboratory Data and CGWAVE Wave Height Estimates along a Transect. ....	102
Figure 27. Wave Phase Diagram for Normal Incident Direction, 100-second Period Wave Condition. ....	104
Figure 28. Estimated Wave Height Diagram for Normal Incident Direction, 100-second Period Wave Condition.....	105

Figure 29. Wave Phase Diagram for Normal Incident Direction, 35-second  
Period Wave Condition. ....107

Figure 30. Estimated Wave Height Diagram for Normal Incident Direction,  
35-second Period Wave Condition.....108

# LIST OF TABLES

Table 1. Summary of Input Information, Keyboard-selected Output Option .....	63
Table 2. Model Input Data.....	81
Table 3. Directional Resolutions Used for Model Input.....	82
Table 4. Model Input Data.....	91

# PREFACE

The research described in this report was authorized and funded under Work Unit 32969, “Development of a New Generation Finite Element Harbor Wave Model,” of the Coastal Research Program, sponsored by Headquarters, U.S. Army Corps of Engineers. Administrative responsibility is assigned to the U.S. Army Engineer Waterways Experiment Station (WES) Coastal and Hydraulics Laboratory (CHL), Dr. James R. Houston, Director, and Mr. Charles C. Calhoun, Jr., Assistant Director. Ms. Carolyn M. Holmes, CHL, was the Program Manager, and Dr. Zeki Demirebilek, Navigation and Harbors Division (NHD), CHL, was the Principal Investigator for the work unit. Dr. Demirebilek worked under the administrative supervision of Dr. Martin C. Miller, Chief, Coastal Hydrodynamics Branch, and Mr. Gene E. Chatham, Chief, NHD, CHL.

This report describes the research that has culminated in a state-of-the-art, general-purpose wave predictive model called CGWAVE. Issues that are emphasized in this report include theory and numerical implementation aspects of this model and a set of examples that illustrate the application of CGWAVE to real-world problems. A step-by-step user’s guide is also provided in Section 7 to facilitate the model’s usage in projects.

The study was performed and the report prepared over the period 1 June 1995 through 15 August 1998. Dr. Demirebilek and a team of researchers led by Dr. Vijay Panchang from the University of Maine, Orono, Maine, developed the numerical modeling goals, concepts, and methodology. The University of Maine team included Drs. Bingyi Xu and David Stewart, Messrs. Liuzhi Zhao, Karl Schlenker, Nishchey Chhabra, and Wei Chen. The study team completed development, implementation, and testing of the model. The field validation part of this research was collaborated with Dr. Michele Okihiro and Professor Robert Guza of the Scripps Institution of Oceanography, La Jolla, California.

At the time of publication of this report, Director of WES was Dr. Robert W. Whalin. Commander was COL Robin R. Cababa, EN.

*The contents of this report are not to be used for advertising, publication, or promotional purposes. Citation of trade names does not constitute an official endorsement or approval of the use of such commercial products.*

## Conversion Factors,

# Non-SI to SI Units of Measurement

Non-SI units of measurement used in this report can be converted to SI units as follows:

<b>Multiply</b>	<b>By</b>	<b>To Obtain</b>
acres	4,046.873	square meters
degrees (angle)	0.01745329	radian
feet	0.3048	meters
knots (international)	0.5144444	meters per second
miles (US Statute)	1.6093	kilometers
nautical miles	1.852	kilometers

# 1 INTRODUCTION

Wave climate plays a very important role in all coastal projects. However, in most cases, little (if any) wave data are available for engineering construction and planning. Field observation and physical modeling of waves are extremely difficult, costly, and time-consuming. Buoys are far away from the project site, and remote-sensing instruments do not systematically provide wave data at the desired resolution in the near shore region. Since no data-recording instrument can anticipate future sea states, the desired sea-state information may be obtained and plans evaluated with reliable mathematical modeling techniques.

It is essential to have reliable information on wave conditions for many coastal and ocean engineering problems. The most important wave conditions for design and assessment in project studies in the area of interest include the wave heights, wave periods and the dominant wave propagation directions. Typically, these wave parameters are obtained from a wave transformation model that transfers the wave data collected at some remote deep water site to the location of the project in the near shore. As waves move from deeper waters to approach the shore, these fundamental wave parameters will change as the wave speed changes and wave energy is redistributed along wave crests due to the depth variation between the transfer sites and the presence of islands, background currents, coastal defense structures, and irregularities of the enclosing shore boundaries and other geological features. Waves undergo the severest change inside the surf zone where wave breaking occurs and in the regions where reflected waves from coastline and structural boundaries interact with the incident waves.

Until recently, the linear wave ray theory was used for wave transformation by tracing rays from deep water to the project site near shore. The effects on wave propagation of the wave height and direction along the wave crest are ignored in the ray theory since this theory assumes that wave energy propagates only along a ray and thus,

energy flux is conserved between two adjacent rays. As a consequence of this assumption, ray theory breaks down when wave ray crossings and caustics occur because the physics of diffraction are totally ignored in the numerical ray models.

Starting in the early 1980's, coastal designers and researchers have recognized the importance of the combined effects of refraction and diffraction and begun to develop improved theories and associated numerical models. There are indeed several wave theories available that could adequately describe the combined refraction and diffraction of waves from deep water to shallow water (Demirbilek and Webster 1992 and 1998). One of these is the mild-slope equation (MSE). This is a depth-averaged, elliptic type partial differential equation which ignores the evanescent modes (locally emanated waves) and assumes that the rate of change of depth and current within a wavelength is small, hence the 'mild-slope' acronym.

Numerous MSE-based numerical models have been developed for predicting the wave forces on offshore structures and studying wave fields around the offshore islands. Numerical, laboratory and field tests of the MSE models have shown that the MSE can provide accurate solutions to problems where the bottom slope is up to 1:3. From a practical standpoint, the computational requirements for solving the MSE are much larger than those for ray tracing. The reasons for this are because the MSE is a two-dimensional equation and has to be solved as a boundary-value problem with appropriate boundary conditions. The entire domain of interest must be discretized and solved simultaneously and the element size has to be small enough that there are about 10 to 15 nodes within each wavelength. These requirements place severe demands on computer resources when applying MSE models to large coastal domains.

A difficult problem in the prediction of waves near shore is to determine where approximately the wave breaking (and breaker line) occurs when waves are inside the surf zone. In numerical models presently used, this location is not known a priori, and is usually selected with an ad hoc criteria based on the ratio of wave height to local water

depth. Bottom friction and dissipation from the surrounding land boundaries (i.e. entrance losses at the mouth of a harbor) may also be empirically incorporated into MSE models. A simplified version of the MSE is known as the 'parabolic approximation' (PA), which usually greatly reduces the excessive computational demands of MSE model at the expense of further assumptions and simplifications which may render the numerical predictions inaccurate and inappropriate for many coastal and ocean engineering problems (Panchang et al. 1998).

The only purpose of adapting the PA is to convert the MSE to a set of simpler equations that describe a wave propagating in a prescribed direction while still taking both refraction and diffraction in the lateral direction into account. The greatest advantage of PA is its numerical efficiency, it can be solved rather easily by numerical means and thus could be used for predicting wave transformation over a relatively large coastal region. When reflection is of major interest, as it is in harbors, the MSE should be used since the PA ignores reflection. One must also be reminded that the PA assumes that the length scale of the wave amplitude variation in the direction of wave propagation (x direction) is much longer than that in the transverse direction (y direction). The PA is derived on the assumption that percentage changes of depth within a typical wavelength are small compared to the wave slope. For details about PA models, see Booij (1981), Liu (1983), Kirby (1983), Liu and Tsay (1984), and Kirby and Dalrymple (1984). The PA has been verified extensively by laboratory studies and field applications (Berkhoff et al. 1982), Liu and Tsay (1984), Kirby and Dalrymple (1984), Vincent and Briggs (1989), (Demirbilek 1994, Demirbilek et al. 1996a and 1996b), and Panchang et al (1998).

The mild-slope wave equation (also known as the "combined refraction-diffraction" equation), first suggested by Eckart (1952) and later re-derived by Berkhoff (1972, 1976) and others, is now well-accepted as the method for estimating coastal wave conditions. It can be used to model a wide spectrum of waves, since it passes, in the limit, to the deep and shallow water equations. Although the equation was developed in the mid-seventies, computational difficulties precluded the development of a model for the

complete mild-slope equation (except for very small domains). Typically, coastal wave propagation problems involve the modeling of very large domains. For example, consider the case of 12 second waves in water of 15 m depth. The wavelength  $L$  is about 136 m; an 8 km by 8 km domain is about  $3600L^2$  in size. The difficulties associated with solving such large problems spawned the development of several simplified models (e.g. the "parabolic approximation" models (Dalrymple et al. 1984; Kirby, 1986), RCPWAVE model (Ebersole, 1985), EVP model (Panchang et al 1988), etc.). However, these simplified models compromised the physics of the mild-slope equation: they model only one- or two-way propagation with weak lateral scattering. Such models are hence applicable only to rectangular water domains for a very limited range of wave directions and frequencies. Most realistic coastal domains with arbitrary wave scattering cannot be modeled with these simplified models.

This manual describes a wave model called CGWAVE developed at the University of Maine under a contract for the U.S. Army Corps of Engineers, Waterways Experiment Station. CGWAVE is a general purpose, state-of-the-art wave prediction model. It is applicable to estimation of wave fields in harbors, open coastal regions, coastal inlets, around islands, and around fixed or floating structures. While CGWAVE simulates the combined effects of wave refraction-diffraction included in the basic mild-slope equation, it also includes the effects of wave dissipation by friction, breaking, nonlinear amplitude dispersion, and harbor entrance losses. CGWAVE is a finite-element model that is interfaced to the SMS model (Jones & Richards, 1992) for graphics and efficient implementation (pre-processing and post-processing). The classical super-element method as well as a new parabolic approximation method developed recently (Xu, Panchang and Demirbilek 1996), are used to treat the open boundary condition. An iterative procedure (conjugate gradient method) introduced by Panchang et al (1991) and modifications suggested by Li (1994) are used to solve the discretized equations, thus enabling the modeler to deal with large domain problems. This manual provides a brief review of the basic theory in Sections 2 and 3, an overview of how this theory is implemented in

Sections 4 through 6, a step by step guide for using this wave model in Section 7, and a set of examples that were run using CGWAVE in Section 8.

## 2 BASIC EQUATIONS

The solution of the two-dimensional elliptic mild-slope wave equation is a well-accepted method for modeling surface gravity waves in coastal areas (e.g. Chen & Houston, 1987; Chen, 1990; Xu & Panchang, 1993; Mei, 1983; Berkhoff, 1976; Kostense et al., 1986; Tsay and Liu, 1983). This equation may be written as:

$$\nabla \cdot (CC_g \nabla \hat{\eta}) + \frac{C_g}{C} \sigma^2 \hat{\eta} = 0 \quad (1)$$

where

$\hat{\eta}(x, y)$  = complex surface elevation function, from which the wave height can be estimated

$\sigma$  = wave frequency under consideration (in radians/second)

$C(x, y)$  = phase velocity =  $\sigma/k$

$C_g(x, y)$  = group velocity =  $\partial \sigma / \partial k = nC$  with

$$n = \frac{1}{2} \left( 1 + \frac{2kd}{\sinh 2kd} \right) \quad (2)$$

$k(x, y)$  = wave number (=  $2\pi/L$ ), related to the local depth  $d(x, y)$  through the linear dispersion relation:

$$\sigma^2 = gk \tanh(kd) \quad (3)$$

Equation 1 simulates wave refraction, diffraction, and reflection (i.e. the general wave scattering problem) in coastal domains of arbitrary shape. However, various other mechanisms also influence the behavior of waves in a coastal area. The mild-slope equation can be modified as follows to include the effects of frictional dissipation (Dalrymple et al 1984; Chen 1986; Liu and Tsay 1985) and wave breaking (Dally et al 1985; De Girolamo et al 1988):

$$\nabla \cdot (CC_g \nabla \hat{\eta}) + \left( \frac{C_g}{C} \sigma^2 + i\sigma w + iC_g \sigma \gamma \right) \hat{\eta} = 0 \quad (4)$$

where  $w$  is a friction factor and  $\gamma$  is a wave breaking parameter. Following Dalrymple et al. (1984), we have used the following form of the damping factor in CGWAVE:

$$w = \left( \frac{2n\sigma}{k} \right) \left[ \frac{2f_r}{3\pi} \frac{ak^2}{(2kd + \sinh 2kd) \sinh kd} \right] \quad (5)$$

where  $a$  ( $= H/2$ ) is the wave amplitude and  $f_r$  is a friction coefficient to be provided by the user. The coefficient  $f_r$  depends on the Reynolds number and the bottom roughness and may be obtained from Madsen (1976) and Dalrymple et al. (1984). Typically, values for  $f_r$  are in the same range as for Manning's dissipation coefficient 'n'. Specifying  $f_r$  as a function of  $(x,y)$  allows the modeler to assign larger values for elements near harbor entrances to simulate entrance loss. For the wave breaking parameter  $\gamma$ , we use the following formulation (Dally et al 1985, Demirbilek 1994, Demirbilek et al. 1996b):

$$\gamma = \frac{\chi}{d} \left( 1 - \frac{\Gamma^2 d^2}{4a^2} \right) \quad (6)$$

where  $\chi$  is a constant (a value of 0.15 is used in CGWAVE following Dally et al (1985)) and  $\Gamma$  is an empirical constant (a value of 0.4 is used in CGWAVE).

In addition to the above mechanisms, nonlinear waves may be simulated in the MSE. This is accomplished by incorporating amplitude-dependent wave dispersion, which has been shown to be important in certain situations (Kirby and Dalrymple 1986). The nonlinear dispersion relation used in place of Equation 3 is

$$\sigma^2 = gk[1 + (ka)^2 F_1 \tanh^5 kd] \tanh\{kd + kaF_2\} \quad (7)$$

where

$$\left. \begin{aligned} F_1 &= \frac{\cosh(4kd) - 2 \tanh^2(kd)}{8 \sinh^4(kd)} \\ F_2 &= \left( \frac{kd}{\sinh(kd)} \right)^4 \end{aligned} \right\} \quad (8)$$

### 3 BOUNDARY CONDITIONS

Along rigid, impermeable vertical walls, no flow normal to the surface gives  $\partial \hat{\eta} / \partial n = 0$ . However, in general, the following partial reflection boundary condition applies along coastlines or permeable structures

$$\frac{\partial \hat{\eta}}{\partial n} = \alpha \hat{\eta} \quad (9)$$

where  $\alpha = \alpha_1 + i\alpha_2$  is a complex coefficient . For simplicity,  $\alpha$  is generally represented as

$$\alpha = ik \frac{1 - K_r}{1 + K_r} \quad (10)$$

where  $K_r$  is the reflection coefficient (Tsay and Liu, 1983; Chen and Houston 1987).

Along the open boundary where outgoing waves must propagate to infinity, the Sommerfeld radiation condition applies

$$\lim_{kr \rightarrow \infty} \sqrt{kr} \left( \frac{\partial}{\partial r} - ik \right) \hat{\eta}_s \rightarrow 0 \quad (11)$$

where  $\hat{\eta}_s$  is the scattering wave potential. It is shown in Mei (1983) that the desired scattered wave potential  $\hat{\eta}_s$ , which is a solution of the mild-slope equation and satisfies the radiation condition Equation 11, can be written as:

$$\hat{\eta}_s = \sum_{n=0}^{\infty} H_n(kr) (\alpha_n \cos n\theta + \beta_n \sin n\theta) \quad (12)$$

where  $H_n(kr)$  are the Hankel functions of the first kind. The Hankel functions of the second kind do not satisfy the Sommerfeld radiation condition at infinity and are hence excluded from (12).

However, the  $\eta_s$  given in (12) requires that the exterior domain be of constant depth. Also for harbor problems (Figure 1), the scattered wave potential as described by (12) demands straight, collinear and fully reflective coastlines in the exterior region. To overcome these problems, Xu, Panchang and Demirebilek (1996) have developed an alternative scheme in dealing with the open boundary condition. This consists of using the following parabolic approximation along the open boundary :

$$\frac{\partial \hat{\eta}_s}{\partial r} + p \hat{\eta}_s + q \frac{\partial \hat{\eta}_s^2}{\partial \theta^2} = 0 \quad (13)$$

where

$$p = \frac{k^2 r^2 + k_0^2 r^2 + ik_0 r + \frac{1}{4}}{2ik_0 r^2} \quad \text{and} \quad q = \frac{1}{2ik_0 r^2} \quad (14)$$

In Equation 14,  $k_0$  can be taken as the wave number corresponding to the averaged water depth along the open boundary  $\Gamma$ . Within the model domain  $\Omega$ , the mild-slope equation applies. The parabolic approximation (13) will be used only along the semi-circular arc  $\Gamma$  as the open boundary condition. The actual implementation of these boundary conditions is described later.

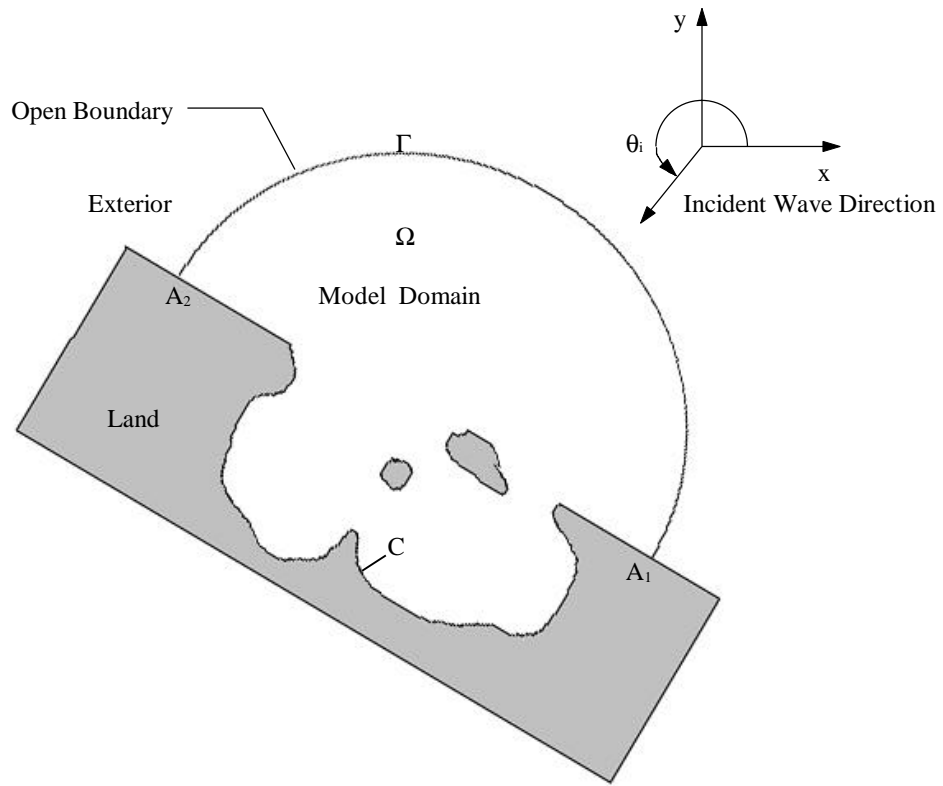


Figure 1. Definition sketch of model domain

# 4 FINITE ELEMENT FORMULATION

## 4.1 Open Sea Problems

CGWAVE uses the finite-element method, which is a powerful approach for modeling coastal phenomena in regions of complex shape. In the case of a group of scatterers surrounded by an open sea of constant depth, the incident wave may be written as (Demirbilek and Gaston, 1985)

$$\hat{\eta}_I = Ae^{ikr \cos(\theta - \theta_I)} = A \sum_{n=0}^{\infty} \epsilon_n i^n J_n(kr) \cos n(\theta - \theta_I) \quad (15)$$

where  $A$  is the amplitude of the incident wave,  $\theta_I$  is the incident wave angle with respect to the  $x$ -axis,  $J_n$  is the  $n$ -th order Bessel functions of the first kind and

$$\epsilon_n = \begin{cases} 1 & \text{when } n = 0 \\ 2 & \text{when } n \neq 0 \end{cases} \quad (16)$$

The incident direction is defined such that the incident wave travels in the positive  $x$ -direction when  $\theta_I$  is equal to zero; the  $x$ -direction is obtained from the bathymetry data file that is input to the CGWAVE program. This bathymetry file should be oriented such that the  $x$ -axis points to the east.

As shown in Figure 2, the entire domain is separated into two sub-domains. Domain  $\Omega$  is the numerical model domain. Domain  $\Omega_0$  is the exterior domain extending to infinity. We assume that complicated topography, structures, and islands, are located inside the circular boundary  $\Gamma$  (in domain  $\Omega$ ). In  $\Omega_0$ , the total wave potential can be written as the sum of incident wave potential and the scattered wave potential:

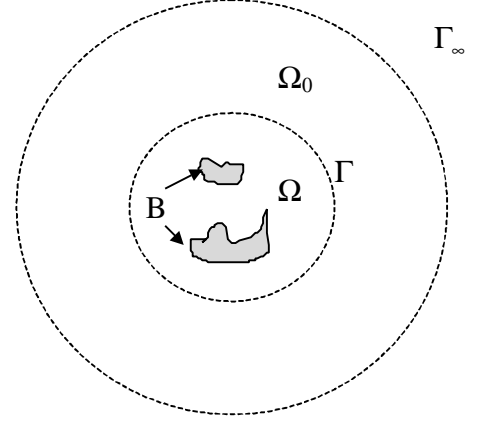


Fig. 2 Definition sketch

$$\hat{\eta}_{\text{ext}} = \hat{\eta}_I + \hat{\eta}_S \quad (17)$$

For brevity, we write the governing Equation 4 in the general form:

$$\nabla \cdot (\tilde{a} \nabla \hat{\eta}) + \tilde{b} \hat{\eta} = 0 \quad (18)$$

where  $\tilde{a} \equiv CC_g$  and  $\tilde{b} \equiv \frac{C_g}{C} \sigma^2 + i\sigma w + iC_g \sigma \gamma$ .

Mei (1983) has shown that the problem of solving Equation 18 with boundary conditions described by (9) on coastlines/structures and by Equation 11 at infinity is equivalent to the stationary of the following functional J:

$$\begin{aligned} J = & \iint_{\Omega} \frac{1}{2} [\tilde{a} (\nabla \hat{\eta})^2 - \tilde{b} \hat{\eta}^2] dA - \int_B \frac{1}{2} \alpha \tilde{a} \hat{\eta}^2 ds + \\ & \int_{\Gamma} \tilde{a} \left[ \left( \frac{1}{2} \hat{\eta}_S + \hat{\eta}_I \right) \frac{\partial \hat{\eta}_S}{\partial n} - \hat{\eta} \frac{\partial (\hat{\eta}_S + \hat{\eta}_I)}{\partial n} \right] ds \end{aligned} \quad (19)$$

The solution of the wave potential can be found by minimizing J over domain  $\Omega$ .

In the finite-element method, we first discretize the computational domain  $\Omega$  into a network of simple triangular elements. The size of these elements should be much smaller than both the local wavelength and the scale of local bathymetric variation. Finer resolution is also desirable at places where the change of amplitude in space is rapid (e.g. near “caustics”). Over each triangular element, the wave potential  $\hat{\eta}$  is approximated by the following linear two-dimensional function  $\hat{\eta}^e$ ,

$$\hat{\eta}^e = \sum_{i=1}^3 N_i^e \hat{\eta}_i^e = [N_1^e + N_2^e + N_3^e] \begin{Bmatrix} \hat{\eta}_1^e \\ \hat{\eta}_2^e \\ \hat{\eta}_3^e \end{Bmatrix} \quad (20)$$

where  $\hat{\eta}_i^e$  represent the wave potentials at the corners (nodes) of the element  $e$  (Figure 3) and  $N_i^e$  are the linear interpolation functions:

$$N_i^e = \frac{a_i + b_i x + c_i y}{2\Delta^e} \quad (21)$$

with

$$\left. \begin{aligned} a_i &= x_j y_k - y_j x_k \\ b_i &= y_j - y_k \\ c_i &= x_k - x_j \end{aligned} \right\} \quad (22)$$

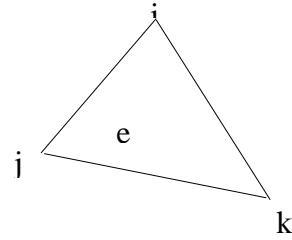


Fig. 3 A typical element

and

$$\begin{aligned} \Delta^e &= \text{area of element } e \\ &= \frac{1}{2} \begin{vmatrix} 1 & x_1^e & y_1^e \\ 1 & x_2^e & y_2^e \\ 1 & x_3^e & y_3^e \end{vmatrix} \end{aligned} \quad (23)$$

Note that for future use, we give

$$\iint_e N_m^e dx dy = \frac{\Delta^e}{3}$$

$$\iiint_e N_i^e N_j^e N_k^e dx dy = \begin{cases} \frac{6}{60} \Delta^e, & i = j = k \\ \frac{2}{60} \Delta^e, & i = j \text{ or } i = k \text{ or } j = k \\ \frac{1}{60} \Delta^e, & i \neq j \neq k \end{cases}$$

Notice that in the above formulations, (i, j, k) are denoted in a counter-clockwise manner.

For element e, the following relations can be established for substitution into (19):

$$\nabla \hat{\eta}^e = \bar{i} \sum_{i=1}^3 \hat{\eta}_i^e \frac{\partial N_i^e}{\partial x} + \bar{j} \sum_{i=1}^3 \hat{\eta}_i^e \frac{\partial N_i^e}{\partial y} \quad (24)$$

$$\begin{aligned} (\nabla \hat{\eta}^e)^2 &= \nabla \hat{\eta}^e \cdot \nabla \hat{\eta}^e \\ &= \left( \sum_{i=1}^3 \hat{\eta}_i^e \frac{\partial N_i^e}{\partial x} \right)^2 + \left( \sum_{i=1}^3 \hat{\eta}_i^e \frac{\partial N_i^e}{\partial y} \right)^2 \\ &= \left\{ \hat{\eta}^e \right\}^T \begin{bmatrix} \left( \frac{\partial N_1^e}{\partial x_a} \right)^2 & \left( \frac{\partial N_1^e}{\partial x_a} \frac{\partial N_2^e}{\partial x_a} \right) & \left( \frac{\partial N_1^e}{\partial x_a} \frac{\partial N_3^e}{\partial x_a} \right) \\ \left( \frac{\partial N_2^e}{\partial x_a} \frac{\partial N_1^e}{\partial x_a} \right) & \left( \frac{\partial N_2^e}{\partial x_a} \right)^2 & \left( \frac{\partial N_2^e}{\partial x_a} \frac{\partial N_3^e}{\partial x_a} \right) \\ \left( \frac{\partial N_3^e}{\partial x_a} \frac{\partial N_1^e}{\partial x_a} \right) & \left( \frac{\partial N_3^e}{\partial x_a} \frac{\partial N_2^e}{\partial x_a} \right) & \left( \frac{\partial N_3^e}{\partial x_a} \right)^2 \end{bmatrix} \left\{ \hat{\eta}^e \right\} \end{aligned} \quad (25)$$

and

$$\begin{aligned}
(\hat{\eta}^e)^2 &= \left( \sum_{i=1}^3 N_i^e \hat{\eta}_i^e \right)^2 \\
&= \{\hat{\eta}^e\}^T \begin{bmatrix} (N_1^e)^2 & (N_1^e N_2^e) & (N_1^e N_3^e) \\ (N_2^e N_1^e) & (N_2^e)^2 & (N_2^e N_3^e) \\ (N_3^e N_1^e) & (N_3^e N_2^e) & (N_3^e)^2 \end{bmatrix} \{\hat{\eta}^e\}
\end{aligned} \tag{26}$$

where  $\alpha = 1, 2$  is the dummy-index notation and  $(x_1 \equiv x, x_2 \equiv y)$ , i.e. Equation 25 represents the sum for  $\alpha = 1$  and  $\alpha = 2$ . Note that  $\{\hat{\eta}^e\}^T = [\hat{\eta}_1^e \hat{\eta}_2^e \hat{\eta}_3^e]$  from Equation 20.

We may also assume that the coefficients  $(\tilde{a}, \tilde{b})$  in Equation 19 vary linearly on element  $e$ :

$$\tilde{a}^e = \sum_{i=1}^3 N_i^e \tilde{a}_i^e, \quad \tilde{b}^e = \sum_{i=1}^3 N_i^e \tilde{b}_i^e \tag{27}$$

For the first part of Equation 19, we may write

$$\begin{aligned}
I_1 &= \iint_{\Omega} \frac{1}{2} (\tilde{a}(\nabla \hat{\eta})^2 - \tilde{b} \hat{\eta}^2) dA \\
&= \frac{1}{2} \sum_{e \in W} \{\hat{\eta}^e\}_{1 \times 3}^T [\mathbf{K}_1^e]_{3 \times 3} \{\hat{\eta}^e\}_{3 \times 1}
\end{aligned} \tag{28}$$

where

$$\mathbf{K}_{1,i,j}^e = \tilde{a}_\beta^e \iint_e N_\beta^e \left( \frac{\partial N_i^e}{\partial x_\alpha} \frac{\partial N_j^e}{\partial x_\alpha} \right) dx dy - \tilde{b}_\beta^e \iint_e N_\beta^e N_i^e N_j^e dx dy \tag{29}$$

where  $\beta = 1, 2, 3$  is another dummy-index notation. Since

$$\frac{\partial N_i^e}{\partial x_\alpha} \frac{\partial N_j^e}{\partial x_\alpha} = \frac{1}{(2\Delta^e)^2} (b_i b_j + c_i c_j) \quad (30)$$

and

$$\iint_e N_\beta^e dx dy = \frac{\Delta^e}{3} \quad (31)$$

we have

$$\tilde{a}_\beta^e \iint_e N_\beta^e \left( \frac{\partial N_i^e}{\partial x_\alpha} \frac{\partial N_j^e}{\partial x_\alpha} \right) dx dy = \frac{\tilde{a}_1^e + \tilde{a}_2^e + \tilde{a}_3^e}{12\Delta^e} (b_i b_j + c_i c_j) \quad (32)$$

The second term of Equation 29 is

$$\begin{aligned} & \tilde{b}_\beta^e \iint_e N_\beta^e N_i^e N_j^e dx dy \\ &= \tilde{b}_i^e \iint_e (N_i^e)^2 N_j^e dx dy + \tilde{b}_j^e \iint_e N_i^e (N_j^e)^2 dx dy + \tilde{b}_k^e \iint_e N_i^e N_j^e N_k^e dx dy \\ &= \frac{\Delta^e}{60} (2\tilde{b}_i^e + 2\tilde{b}_j^e + \tilde{b}_k^e) \end{aligned} \quad (33)$$

for  $i \neq j$ , and

$$\begin{aligned}
& \tilde{b}_\beta^e \iint_e N_\beta^e N_i^e N_j^e dx dy \\
&= \tilde{b}_i^e \iint_e (N_i^e)^3 dx dy + \tilde{b}_{k1}^e \iint_e N_{k1}^e (N_i^e)^2 dx dy + \tilde{b}_{k2}^e \iint_e N_{k2}^e (N_i^e)^2 dx dy \\
&= \frac{\Delta^e}{30} (3\tilde{b}_i^e + \tilde{b}_{k1}^e + \tilde{b}_{k2}^e)
\end{aligned} \tag{34}$$

for  $i = j \equiv i$ , where  $k1$  &  $k2$  are the other two nodes of element  $e$ . Now, Equation 29 can be written as

$$\begin{aligned}
\mathbf{K}_{i,i,j}^e &= \frac{\tilde{a}_1 + \tilde{a}_2 + \tilde{a}_3}{12\Delta^e} (\mathbf{b}_i \mathbf{b}_j + \mathbf{c}_i \mathbf{c}_j) - \\
&\begin{cases} \frac{\Delta^e}{60} (2\tilde{b}_i^e + 2\tilde{b}_j^e + \tilde{b}_k^e) & \text{when } i \neq j \\ \frac{\Delta^e}{30} (3\tilde{b}_i^e + \tilde{b}_{k1}^e + \tilde{b}_{k2}^e) & \text{when } i = j \equiv i \end{cases}
\end{aligned} \tag{35}$$

After computing the element matrix  $[\mathbf{K}_i^e]$  for all the elements ( $e = 1, 2, 3, \dots, E$ ), where  $E$  is the total number of elements, we can assemble them into a “global” matrix  $[\mathbf{K}_1]$ . Equation 28 becomes

$$\mathbf{I}_1 = \frac{1}{2} \sum_{e \in \Omega} \left\{ \hat{\eta}^e \right\}_{1 \times 3}^T \left[ \mathbf{K}_i^e \right]_{3 \times 3} \left\{ \hat{\eta}^e \right\}_{3 \times 1} = \frac{1}{2} \left\{ \hat{\eta} \right\}^T [\mathbf{K}_1] \left\{ \hat{\eta} \right\} \tag{36}$$

In (36)

$$\left\{ \hat{\eta} \right\}^T = \left\{ \hat{\eta}_1, \hat{\eta}_2, \hat{\eta}_3, \dots, \dots, \hat{\eta}_N \right\} \tag{37}$$

where  $N$  is the total number of nodes in domain  $\Omega$

The second part of Equation 19 is

$$I_2 = \int_B \frac{1}{2} \alpha \tilde{a} \hat{\eta}^2 ds \quad (38)$$

where B denotes all the coastline and internal land boundaries.

Along a segment p of the coastal boundaries B (Figure 4), the wave surface elevation function  $\hat{\eta}$  and the variable  $\tilde{a}$  are approximated by linear functions as before:

$$\hat{\eta}^p = N_i^p \hat{\eta}_i^p + N_j^p \hat{\eta}_j^p \quad (39)$$

$$\tilde{a}^p = N_i^p \tilde{a}_i^p + N_j^p \tilde{a}_j^p \quad (40)$$

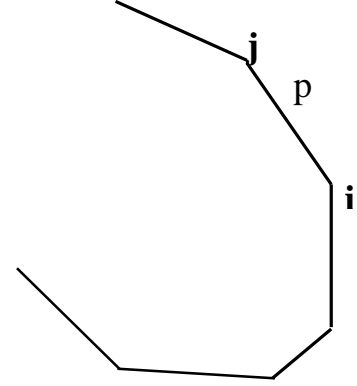


Figure 4. Boundary segments

Here, we assume that  $i \rightarrow j$  is the positive direction of the boundary, counter-clockwise for the coastline boundaries and clockwise for internal land boundaries.

First, let us find the expression for  $(\hat{\eta}^p)^2$  on segment P:

$$\begin{aligned} (\hat{\eta}^p)^2 &= (N_i^p \hat{\eta}_i^p + N_j^p \hat{\eta}_j^p)^2 \\ &= \begin{Bmatrix} \hat{\eta}_i^p, & \hat{\eta}_j^p \end{Bmatrix} \begin{bmatrix} (N_i^p)^2 & (N_i^p N_j^p) \\ (N_j^p N_i^p) & (N_j^p)^2 \end{bmatrix} \begin{pmatrix} \hat{\eta}_i^p \\ \hat{\eta}_j^p \end{pmatrix} \end{aligned} \quad (41)$$

Equation 38 can then be written as

$$\begin{aligned}
I_2 &= \int_B \frac{1}{2} \alpha \tilde{a} \hat{\eta}^2 ds \\
&= \frac{1}{2} \sum_{P=1}^{N_b-1} \{ \hat{\eta}_i^P, \hat{\eta}_j^P \} [K_2^P] \begin{pmatrix} \hat{\eta}_i^P \\ \hat{\eta}_j^P \end{pmatrix}
\end{aligned} \tag{42}$$

where  $N_b$  is the total number of nodes along boundary B and

$$\begin{aligned}
K_{2,i,j}^P &= \alpha \tilde{a}_b^P \int_{(\text{point } i)}^{(\text{point } j)} N_b^P N_i^P N_j^P ds \\
&= \begin{cases} \frac{1}{12} \alpha L^P (\tilde{a}_i^P + \tilde{a}_j^P) & \text{for } i \neq j \\ \frac{1}{12} \alpha L^P (3\tilde{a}_i^P + \tilde{a}_j^P) & \text{for } i = j \equiv i \end{cases}
\end{aligned} \tag{43}$$

Assembling all segments on coastal boundary B, we have

$$I_2 = \frac{1}{2} \sum_{P=1}^{N_b-1} \{ \hat{\eta}_i^P, \hat{\eta}_j^P \} [K_2^P] \begin{pmatrix} \hat{\eta}_i^P \\ \hat{\eta}_j^P \end{pmatrix} = \frac{1}{2} \{ \hat{\eta}^B \}^T \begin{matrix} [K_2] \\ 1 \times N_b & N_b \times N_b & N_b \times 1 \end{matrix} \{ \hat{\eta}^B \} \tag{44}$$

The third part integral in Equation 19 is

$$\begin{aligned}
&\int_G \tilde{a} \left[ \left( \frac{1}{2} \hat{\eta}_s + \hat{\eta}_I \right) \frac{\partial \hat{\eta}_s}{\partial n} - \hat{\eta} \frac{\partial (\hat{\eta}_s + \hat{\eta}_I)}{\partial n} \right] ds = I_3 + I_4 + I_5 + I_6 \\
I_3 &= \frac{1}{2} \int_G \tilde{a} \hat{\eta}_s \frac{\partial \hat{\eta}_s}{\partial n} ds \\
I_4 &= - \int_G \tilde{a} \hat{\eta} \frac{\partial \hat{\eta}_s}{\partial n} ds \quad \cdots \quad I_4 \\
I_5 &= - \int_G \tilde{a} \hat{\eta} \frac{\partial \hat{\eta}_I}{\partial n} ds \quad \cdots \quad I_5 \\
I_6 &= + \int_G \tilde{a} \hat{\eta}_I \frac{\partial \hat{\eta}_s}{\partial n} ds \quad \cdots \quad I_6
\end{aligned} \tag{45}$$

For simplicity, the open boundary  $\Gamma$  is assumed to be a circle of radius  $R$ . For computational purposes, the series for the scattered waves (Equation 12) and the series for incident waves (Equation 15) are truncated after a finite number of terms. In principle, trial and error should be performed in modeling a certain case in order to choose the appropriate number of terms. Here, we assume that the series will be truncated after  $m$  terms.

By using the orthogonality of trigonometric functions:

$$\int_0^{2\pi} \sin n\theta \sin m\theta d\theta = \begin{cases} 0 & \text{when } n \neq m \\ \pi & \text{when } n = m \end{cases} \quad (46)$$

$$\int_0^{2\pi} \cos n\theta \cos m\theta d\theta = \begin{cases} 0 & \text{when } n \neq m \\ \pi & \text{when } n = m \neq 0 \\ 2\pi & \text{when } n = m = 0 \end{cases} \quad (47)$$

and substituting  $\hat{\eta}_s$  with Equation 12, the line integral  $I_3$  in Equation 45 can be evaluated analytically, as follows

$$I_3 = \frac{\pi}{2} kR \tilde{a} \left[ 2\alpha_0^2 H_0 H_0' + \sum_{n=1}^m (\alpha_n^2 + \beta_n^2) H_n H_n' \right] \quad (48)$$

where  $k$  and  $\tilde{a}$  can be taken as average values along  $\Gamma$  and

$$H_n \equiv H_n^{(1)}(kR), \quad H_n' \equiv \left[ \frac{d}{d(kr)} H_n^{(1)}(kr) \right]_{r=R} \quad (49)$$

For convenience of mathematical manipulation later on, we define the following vector for the unknown coefficients  $\alpha_i$  and  $\beta_i$  :

$$\{\boldsymbol{\mu}\}_{1 \times M}^T = \{\alpha_0, \alpha_1, \beta_1, \alpha_2, \beta_2, \dots, \alpha_m, \beta_m\} \quad (50)$$

where  $M = 2m + 1$ . The integral  $I_3$  can now be rewritten as

$$I_3 = \frac{1}{2} \{\boldsymbol{\mu}\}^T [\mathbf{K}_3] \{\boldsymbol{\mu}\} \quad (51)$$

where  $[\mathbf{K}_3]$  is a diagonal matrix of dimension  $M$  by  $M$ :

$$[\mathbf{K}_3] = \pi k R \tilde{a} \text{diag} \{2H'_0 H_0, H'_1 H_1, H'_1 H_1, \dots, H'_m H_m, H'_m H_m\} \quad (52)$$

The integral  $I_4$  in Equation 45 is

$$\begin{aligned} I_4 &= \int_G \tilde{a} \hat{\eta} \frac{\partial \hat{\eta}_s}{\partial n} ds \\ &\cong k \tilde{a} \sum_{P=1}^{N_\Gamma} \int_{\text{segment } P} (N_i^P \hat{\eta}_i^P + N_j^P \hat{\eta}_j^P) \left[ \alpha_0 H'_0 + \sum_{n=0}^m H'_n (\alpha_n \cos n \theta_P + \beta_n \sin n \theta_P) \right] ds \\ &= \frac{k \tilde{a}}{2} \sum_{P=1}^{N_\Gamma} L^P (\hat{\eta}_i^P + \hat{\eta}_j^P) \left[ \alpha_0 H'_0 + \sum_{n=0}^m H'_n (\alpha_n \cos n \theta_P + \beta_n \sin n \theta_P) \right] \end{aligned} \quad (53)$$

where  $L^P$  is the length of segment  $P$  and  $N_\Gamma$  is the total number of segments (= total number of nodes) along the circular boundary  $\Gamma$  (Figure 5). In Equation 53, the value of  $\partial \hat{\eta}_s / \partial n$  is approximated by its value at the center of segment  $P$ . Equation 53 may be written in matrix form :

$$I_4 = \{\hat{\mathbf{h}}^\Gamma\}^T [\mathbf{K}_4] \{\mathbf{m}\} \quad (54)$$

where  $\{\hat{\eta}^\Gamma\}$  is the subset of  $\{\hat{\eta}\}$  for nodes situated on boundary  $\Gamma$  :

$$\{\hat{\eta}^\Gamma\}_{1 \times N_\Gamma}^T = \{\hat{\eta}_1^\Gamma, \hat{\eta}_2^\Gamma, \hat{\eta}_3^\Gamma, \dots, \hat{\eta}_{N_\Gamma}^\Gamma\} \quad (55)$$

and  $[K_4]$  is a fully populated  $N_\Gamma \times M$  matrix :

$$[K_4] = \frac{k\tilde{a}}{2} \times \begin{bmatrix} 2H_0' L^1 \cdots H_n'(\cos n\theta_{N_\Gamma-1} + \cos n\theta_1)L^1 & H_n'(\sin n\theta_{N_\Gamma-1} + \sin n\theta_1)L^1 & \cdots \\ 2H_0' L^2 \cdots H_n'(\cos n\theta_1 + \cos n\theta_2)L^2 & H_n'(\sin n\theta_1 + \sin n\theta_2)L^2 & \cdots \\ \cdot & \cdot & \cdot \\ \cdot & \cdot & \cdot \\ \cdot & \cdot & \cdot \\ 2H_0' L^{N_\Gamma} \cdots H_n'(\cos n\theta_{N_\Gamma-1} + \cos n\theta_{N_\Gamma})L^{N_\Gamma} & H_n'(\sin n\theta_{N_\Gamma-1} + \sin n\theta_{N_\Gamma})L^2 & \cdots \end{bmatrix} \quad (56)$$

where  $n = 1, 2, \dots, m$ .

The next integral in Equation 45 is  $I_5$ . Similar to the treatment in  $I_4$ , we will take the center value of  $\partial \hat{\eta}_I / \partial n$  and assume linear variation of  $\hat{\eta}$  for a segment on boundary  $\Gamma$ . Substituting  $\hat{\eta}_I$  in  $I_5$  by Equation 15, it is easy to find

$$\begin{aligned} I_5 &= \int_\Gamma \tilde{a} \hat{\eta} \frac{\partial \hat{\eta}_I}{\partial n} ds \\ &= \frac{i}{2} k \tilde{a} A \sum_{p=1}^{N_\Gamma} L^p (\hat{\eta}_i^p + \hat{\eta}_j^p) \cos(\theta_p - \theta_1) \exp[ikR \cos(\theta_p - \theta_1)] \\ &= \{Q_5\}^T \{\hat{\eta}^\Gamma\} \end{aligned} \quad (57)$$

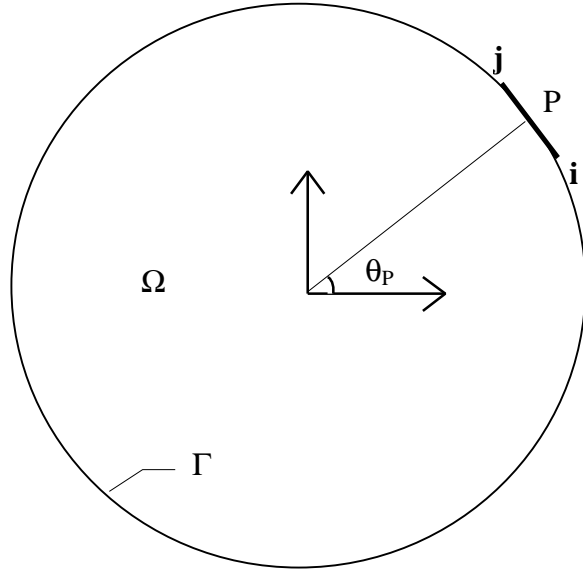


Figure 5. Definition sketch for line integrals along the open boundary  $\Gamma$

where

$$\{Q_5\}^T = \frac{i}{2} k \tilde{a} A \left\{ (q_{N_\Gamma} + q_1) L^1, (q_1 + q_2) L^2, \dots, (q_{N_\Gamma-1} + q_{N_\Gamma}) L^{N_\Gamma} \right\} \quad (58)$$

and

$$q_P = \cos(\theta_P - \theta_1) \exp[ikR \cos(\theta_P - \theta_1)], \quad P = 1, 2, \dots, N_\Gamma \quad (59)$$

The last integral  $I_6$  in Equation 45 involves both  $\hat{\eta}_S$  and  $\hat{\eta}_I$ . Here, the Bessel-Fourier form of  $\hat{\eta}_I$  (see Equation 15) will be used and the integral can be found analytically:

$$\begin{aligned} I_6 &= \int_G \tilde{a} \hat{\eta}_I \frac{\partial \hat{\eta}_S}{\partial n} ds \\ &= k \tilde{a} A \int_\Gamma \sum_{n=0}^m \epsilon_n i^n J_n(kr) \cos n(\theta - \theta_1) \sum_{n=0}^m H_n'(\alpha_n \cos n\theta + \beta_n \sin n\theta) ds \\ &= k \tilde{a} A \int_0^{2\pi} \sum_{n=0}^m \epsilon_n i^n J_n(kr) \cos n(\theta - \theta_1) \sum_{n=0}^m H_n'(\alpha_n \cos n\theta + \beta_n \sin n\theta) R d\theta \\ &= \{Q_6\}^T \{\mu\} \end{aligned} \quad (60)$$

where

$$\begin{aligned} \{Q_6\}^T &= 2\pi k R \tilde{a} A \times \\ &\left\{ J_0 H_0', i J_1 H_1' \cos \theta_1, i J_1 H_1' \sin \theta_1, \dots, i^m J_m H_m' \cos m\theta_1, i^m J_m H_m' \sin m\theta_1 \right\} \end{aligned} \quad (61)$$

Now, we have evaluated all the integrals of the functional  $J$  defined by Equation 19 using a linear triangular element network. Collecting these integrals together, we have

$$\begin{aligned}
J &\equiv I_1 - I_2 + I_3 - I_4 - I_5 + I_6 \\
&= \frac{1}{2} \{\hat{\eta}\}^T [\mathbf{K}_1] \{\hat{\eta}\} - \frac{1}{2} \{\hat{\eta}^B\}^T [\mathbf{K}_2] \{\hat{\eta}^B\} + \frac{1}{2} \{\mu\}^T [\mathbf{K}_3] \{\mu\} \\
&\quad - \{\hat{\eta}^\Gamma\}^T [\mathbf{K}_4] \{\mu\} - \{\mathbf{Q}_5\}^T \{\hat{\eta}^\Gamma\} + \{\mathbf{Q}_6\}^T \{\mu\}
\end{aligned} \tag{62}$$

Since J is stationary, the following must be true for the solution of the problem :

$$\frac{\partial J}{\partial \hat{\eta}_i} = 0 \quad i = 1, 2, 3, \dots, N \tag{63}$$

and

$$\frac{\partial J}{\partial \mu_j} = 0 \quad j = 1, 2, 3, \dots, M \tag{64}$$

These relations give

$$[\mathbf{K}_1] \{\hat{\eta}\} - [\mathbf{K}_2] \{\hat{\eta}^B\} - [\mathbf{K}_4] \{\mu\} = \{\mathbf{Q}_5\} \tag{65}$$

and

$$[\mathbf{K}_3] \{\mu\} - [\mathbf{K}_4]^T \{\hat{\eta}^\Gamma\} = -\{\mathbf{Q}_6\} \tag{66}$$

From Equation 66, we have

$$\{\mu\} = -[\mathbf{K}_3]^{-1} \{\mathbf{Q}_6\} + [\mathbf{K}_3]^{-1} [\mathbf{K}_4]^T \{\hat{\eta}^\Gamma\} \tag{67}$$

Substituting  $\{\mu\}$  in Equation 65 by Equation 67, Equation 65 becomes

$$[\mathbf{K}_1]\{\hat{\eta}\} - [\mathbf{K}_2]\{\hat{\eta}^B\} - [\mathbf{K}_4][\mathbf{K}_3]^{-1}[\mathbf{K}_4]^T\{\hat{\eta}^r\} = \{Q_5\} - [\mathbf{K}_4][\mathbf{K}_3]^{-1}\{Q_6\} \quad (68)$$

Finally, after proper assembling, we have

$$[\mathbf{A}]\{\hat{\eta}\} = \{f\} \quad (69)$$

Equation 69 is the desired linear system of equations, which is the finite-element representation of the mild-slope equation for open sea problems. Notice that the boundary conditions, including coastline boundaries and the circular open boundary, are all consolidated in Equation 69. The solution method used in CGWAVE for Equation 69 is described in the next section.

## 4.2 Harbor Problems

The finite-element formulation given above is for open-sea offshore problems. In case of harbor problems, the formulation is analogous. The only difference arises from the treatment of the open boundary condition. The classical treatment of these problems assumes that the coastlines outside the model domain are straight, collinear and fully reflective. The exterior wave field is written as  $\hat{\eta}_{\text{ext}} = \hat{\eta}_I + \hat{\eta}_R + \hat{\eta}_S$ , where  $\hat{\eta}_I$ ,  $\hat{\eta}_R$ , and  $\hat{\eta}_S$  represent the incident, the reflected, and the scattered wave fields, respectively. Based on the assumptions, we define (Demirbilek and Gaston 1985)

$$\begin{aligned} \hat{\eta}_0 &= \hat{\eta}_I + \hat{\eta}_R \\ &= A e^{ikr \cos(\theta - \theta_I)} + A e^{ikr \cos(\theta + \theta_I)} \\ &= 2A \sum_{n=0}^{\infty} \epsilon_n i^n J_n(kr) \cos n \theta_I \cos n \theta \end{aligned} \quad (70)$$

where  $A$  is the incident wave amplitude and  $\theta_I$  is the incident wave angle with respect to

the exterior coastlines as shown in Figure 1. The scattered wave potential  $\hat{\eta}_s$  in the exterior region must take the following form in order to comply with the exterior coastline boundary conditions:

$$\hat{\eta}_s = \sum_{n=0}^{\infty} H_n(kr) \alpha_n \cos n\theta \quad (71)$$

as shown in Xu, Panchang and Demirbilek (1995). The corresponding functional for harbor problems has the same form as Equation 19 except that  $\hat{\eta}_1$  in Equation 19 has to be replaced by  $\hat{\eta}_0$  (Equation 70),  $\hat{\eta}_s$  takes the new form given by Equation 71, and the open boundary  $\Gamma$  represents the semicircle as shown in Figure 1. The finite-element formulation of harbor problems can now readily be found in a manner similar to the open-sea problems described above, by replacing  $\hat{\eta}_1$  and  $\hat{\eta}_s$  with Equation 70 and Equation 71 and performing the boundary integration for  $I_4$  through  $I_6$  from 0 to  $\pi$ .

### 4.3 Alternative Open Boundary Treatment

For most practical cases, the fully reflective straight coastline assumption in the classical treatment of the open boundary condition is improper and the effects may be substantial. Xu, Panchang and Demirbilek (1995) have shown that it is preferable to use the parabolic approximation (Equation 13) as the open boundary condition. For harbor problems, along the open boundary  $\Gamma$  (Figure 1) we use (13) as the boundary condition for the scattered waves. Matching the potential and its normal derivative along  $\Gamma$  and using the parabolic open boundary condition (13), we have the total potential as

$$\hat{\eta} = \hat{\eta}_0 + \hat{\eta}_s \quad (72)$$

and

$$\frac{\partial \hat{\eta}}{\partial n} = \frac{\partial \hat{\eta}_0}{\partial r} + \frac{\partial \hat{\eta}_s}{\partial r} = \frac{\partial \hat{\eta}_0}{\partial r} - \left( p \hat{\eta}_s + q \frac{\partial^2 \hat{\eta}_s}{\partial \theta^2} \right) \quad (73)$$

Using Equation 72 to eliminate  $\hat{\eta}_s$  yields

$$\frac{\partial \hat{\eta}}{\partial n} = -p\hat{\eta} - q \frac{\partial^2 \hat{\eta}}{\partial \theta^2} + g \quad (74)$$

where

$$g = \frac{\partial \hat{\eta}_0}{\partial r} + p\hat{\eta}_0 + q \frac{\partial^2 \hat{\eta}_0}{\partial \theta^2} \quad (75)$$

Equation 74 is the open boundary condition in terms of total wave potential  $\hat{\eta}$ .

For this parabolic boundary problem, the desired Jacobian functional may be more complicated than that of Equation 19. Therefore the Galerkin finite-element formulation is used.

According to the Galerkin approach, the wave potential  $\hat{\eta}$  is approximated by

$$\hat{\eta} = \sum_{i=1}^n \hat{\eta}_i N_i \quad (76)$$

where  $\hat{\eta}_i$  is the solution  $\hat{\eta}$  at node  $i$  and  $N_i(x, y)$  is the linear interpolation function for node  $i$ . The unknown  $\hat{\eta}_i$  can be determined from the orthogonality conditions between function  $N_i$  and left-hand side of Equation 18, that is

$$\iint_{\Omega} (\nabla(\tilde{a}\nabla\hat{\eta}) + \tilde{b}\hat{\eta}) N_i d\Omega = 0 \quad (i = 1, \dots, N) \quad (77)$$

Using the divergence theorem, Equation 77 becomes

$$-\left(\int_C + \int_\Gamma\right) N_i \left( \tilde{a} \frac{\partial \hat{\eta}}{\partial n} \right) ds + \iint_\Omega \tilde{a} \nabla \hat{\eta} \nabla N_i d\Omega + \iint_\Omega \tilde{b} \hat{\eta} \nabla N_i d\Omega = 0 \quad (78)$$

where C and  $\Gamma$  denotes coastal boundaries and open boundaries respectively, and  $\partial \hat{\eta} / \partial n$  is the normal derivative of  $\hat{\eta}$ .

Under the linear assumption, the interpolation function  $N_i$  is to satisfy

$$N_i(x, y) = \begin{cases} 1 & \text{for } (x, y) \text{ at node } i \\ 0 \text{ to } 1 & \text{for } (x, y) \text{ within elements surrounding node } i \\ 0 & \text{for } (x, y) \text{ outside elements surrounding node } i \end{cases} \quad (79)$$

Therefore,  $N_i$  can be represented as

$$N_i(x, y) = \sum_{e_i} N_i^e(x, y) \quad (80)$$

where  $e_i$  refers to those elements around node  $i$  and  $N_i^e(x, y)$  is the linear interpolation function corresponding to an element  $e$  and one of its node  $i$ . When  $(x, y)$  is at boundary, Equation 80 becomes

$$N_i(x, y) = \sum_{P_i} N_i^P(x, y) = N_i^{P_1}(x, y) + N_i^{P_2}(x, y) \quad (81)$$

where  $P_1$  and  $P_2$  are the boundary segments to either side on node  $i$ . The function  $N_i^P \equiv 0$  for all other segments.

Within an element  $e$ , the value of  $\hat{\eta}$  is obtained by substituting (80) into (76),

$$\hat{\eta}(x, y) = \hat{\eta}_i N_i^e + \hat{\eta}_j N_j^e + \hat{\eta}_k N_k^e \quad (82)$$

where  $i(x_i, y_i)$ ,  $j(x_j, y_j)$ ,  $k(x_k, y_k)$  are the three nodes of element  $e$  (see Figure 3) and function  $N_i^e(x, y)$  is given by Equations 21 through 24.

When  $(x, y)$  is on a boundary segment with nodes  $i$  and  $j$  at the ends, Equation 82 is simplified to:

$$\hat{\eta}(x, y) = \hat{\eta}_i N_i^P + \hat{\eta}_j N_j^P \quad (83)$$

where  $N_i^P = (s_j - s) / L^P$ ,  $N_j^P = (s - s_i) / L^P$ , and  $s$  is the relative coordinate along  $P$  and has values of  $s_i$  and  $s_j$  at the two endpoints. The length of the segment is  $L^P = |s_i - s_j|$ .

The following relations referring to linear function  $N_i^e(x, y)$  and  $N_i^P(x, y)$  are developed for later use:

$$\nabla N_i^e = \frac{\partial N_i^e}{\partial x} \hat{i} + \frac{\partial N_i^e}{\partial y} \hat{j} = \frac{1}{2\Delta^e} (b_i \hat{i} + c_i \hat{j}) \quad (84)$$

$$\iint_e N_i^e dx dy = \frac{\Delta^e}{3} \quad (85)$$

$$\iint_e N_i^e N_j^e N_k^e dx dy = \begin{cases} 6\Delta^e / 60 & \text{for } i = j = k \\ 2\Delta^e / 60 & \text{for } i = j \text{ or } j = k \text{ or } k = i \\ \Delta^e / 60 & \text{for } i \neq j \neq k \end{cases} \quad (86)$$

$$\frac{\partial N_i^P}{\partial s} = -\frac{1}{L^P}, \quad \frac{\partial N_j^P}{\partial s} = \frac{1}{L^P} \quad (87)$$



$$\begin{aligned}
\text{III}_i^e &= -\left(\iint_e \tilde{b} N_i^{e2} d\Omega\right) \hat{\eta}_i - \left(\iint_e \tilde{b} N_i^e N_j^e d\Omega\right) \hat{\eta}_j - \left(\iint_e \tilde{b} N_i^e N_k^e d\Omega\right) \hat{\eta}_k \\
&= B_{ii}^e \hat{\eta}_i + B_{ij}^e \hat{\eta}_j + B_{ik}^e \hat{\eta}_k
\end{aligned} \tag{95}$$

$$\text{III}_j^e = B_{ji}^e \hat{\eta}_i + B_{jj}^e \hat{\eta}_j + B_{jk}^e \hat{\eta}_k \tag{96}$$

$$\text{III}_k^e = B_{ki}^e \hat{\eta}_i + B_{kj}^e \hat{\eta}_j + B_{kk}^e \hat{\eta}_k \tag{97}$$

Assuming that the coefficients  $\tilde{a}$  and  $\tilde{b}$  also vary linearly on element  $e$ , i.e.

$$\tilde{a} = \tilde{a}_i N_i^e + \tilde{a}_j N_j^e + \tilde{a}_k N_k^e \tag{99}$$

$$\tilde{b} = \tilde{b}_i N_i^e + \tilde{b}_j N_j^e + \tilde{b}_k N_k^e \tag{100}$$

then using the relations (84), (85) and (86), we have

$$\begin{aligned}
A_{IJ}^e &= \iint_e \tilde{a} \nabla N_I^e \nabla N_J^e d\Omega \\
&= \frac{1}{4\Delta^{e2}} (b_I b_J + c_I c_J) \iint_e \left( \tilde{a}_i N_i^e + \tilde{a}_j N_j^e + \tilde{a}_k N_k^e \right) d\Omega \\
&= \frac{1}{12\Delta^e} \left( \tilde{a}_i + \tilde{a}_j + \tilde{a}_k \right) (b_I b_J + c_I c_J) \quad (I, J = i, j, k)
\end{aligned} \tag{101}$$

$$\begin{aligned}
B_{IJ}^e &= -\iint_e \left( \tilde{b}_i N_i^e + \tilde{b}_j N_j^e + \tilde{b}_k N_k^e \right) N_I^e N_J^e d\Omega \\
&= -\begin{cases} \frac{\Delta^e}{30} \left( \tilde{b}_i + \tilde{b}_j + \tilde{b}_k + 2\tilde{b}_I \right) & \text{for } I = J \\ \frac{\Delta^e}{60} \left( \tilde{b}_i + \tilde{b}_j + \tilde{b}_k + \tilde{b}_I + \tilde{b}_J \right) & \text{for } I \neq J \end{cases} \quad (I, J = i, j, k)
\end{aligned} \tag{102}$$

By combining the expressions for  $\hat{\eta}$  at nodes i, j and k, the second and third terms of Equation 91 for element e can be represented by means of matrix,

$$[\mathbb{II}^e + \mathbb{III}^e] = \left( [A^e] + [B^e] \right) \{ \hat{\eta}^e \} \quad (e = 1, 2, \dots, E) \quad (103)$$

where

$$\{ \hat{\eta}^e \} = \{ \hat{\eta}_i^e, \hat{\eta}_j^e, \hat{\eta}_k^e \}^T \quad (104)$$

and the expression for  $[A^e] + [B^e]$  is the same as that for  $[K_i^e]$ , see Equation 35.

An expression for the first term of Equation 91 may be obtained by applying certain boundary condition and also using Equations 87 through 90. This gives the following relationship when node i is at coastal boundary,

$$\begin{aligned} I_{Ci}^P &= -\alpha \int_P N_i^P \left( \tilde{a}_i N_i^P + \tilde{a}_j N_j^P \right) \left( N_i^P \hat{\eta}_i^P + N_j^P \hat{\eta}_j^P \right) ds \\ &= C_{ii}^P \hat{\eta}_i^P + C_{ij}^P \hat{\eta}_j^P \end{aligned} \quad (105)$$

Similarly for node j,

$$I_{Cj}^P = C_{ji}^P \hat{\eta}_i^P + C_{jj}^P \hat{\eta}_j^P \quad (106)$$

Therefore, for segment P with node i and j, we have the matrix formula

$$[I_C^P] = [C^P] \{ \hat{\eta}^P \} \quad (107)$$

where

$$\{\hat{\eta}^P\} = \{\hat{\eta}_i, \hat{\eta}_j\}^T \quad (108)$$

$$\begin{aligned} C_{II}^P &= -\alpha \int_P \left( \tilde{a}_i N_i^P + \tilde{a}_j N_j^P \right) N_i^P N_j^P ds \\ &= \begin{cases} -\frac{L^P}{12} \alpha (\tilde{a}_i + \tilde{a}_j + 2\tilde{a}_i) & \text{for } I = J \\ -\frac{L^P}{12} \alpha (\tilde{a}_i + \tilde{a}_j) & \text{for } I \neq J \end{cases} \quad (I, J = i, j) \end{aligned} \quad (109)$$

When node  $i$  is at open boundary, boundary condition (Equation 74) applies, and the first term in Equation 91 becomes

$$I_{\Gamma_i}^P = \int_P \tilde{a} \left( p\hat{\eta} + q \frac{\partial^2 \hat{\eta}}{\partial \theta^2} - g \right) N_i^P ds \quad (110)$$

Similar to  $I_C^P$  (Equations 107 and 108), the first term of the  $i^{\text{th}}$  and  $j^{\text{th}}$  Equation in (110) is

$$[I_{\Gamma_i}^P] = [\Gamma_i^P] \{\hat{\eta}^P\} \quad (111)$$

where

$$\Gamma_{I_u}^P = \begin{cases} \frac{L^P}{12} p (\tilde{a}_i + \tilde{a}_j + 2\tilde{a}_i) & \text{for } I = J \\ \frac{L^P}{12} p (\tilde{a}_i + \tilde{a}_j) & \text{for } I \neq J \end{cases} \quad (I, J = i, j) \quad (112)$$

The second terms in (110) are

$$\begin{aligned} I_{\Gamma_{2i}}^P &= \int_P \tilde{a} q r^2 \frac{\partial^2 \hat{\eta}}{\partial s^2} N_i^P ds = \tilde{a} q r^2 \left( N_i^P \frac{\partial \hat{\eta}}{\partial s} \Big|_i^j - \int_P \frac{\partial \hat{\eta}}{\partial s} \frac{\partial N_i}{\partial s} ds \right) \\ &= -\tilde{a} q r^2 \frac{\partial \hat{\eta}}{\partial s} \Big|_i - \frac{\tilde{a} q r^2}{L_P} (\hat{\eta}_i - \hat{\eta}_j) \end{aligned} \quad (113)$$

and

$$I_{\Gamma_{2j}}^P = \tilde{a} q r^2 \frac{\partial \hat{\eta}}{\partial s} \Big|_j - \frac{\tilde{a} q r^2}{L_P} (\hat{\eta}_j - \hat{\eta}_i) \quad (114)$$

where  $r$  is the radius of the semicircle. These terms can also be written in matrix form as

$$[I_{\Gamma_2}^P] = [\Gamma_2^P] \{\hat{\eta}^P\} + [D^P] \quad (115)$$

where

$$[\Gamma_2^P] = -\frac{\tilde{a} q r^2}{L^P} \begin{bmatrix} 1 & -1 \\ -1 & 1 \end{bmatrix} \quad (116)$$

and

$$[D^P] = -\tilde{a} q r^2 \left\{ \frac{\partial \hat{\eta}}{\partial s_i}, -\frac{\partial \hat{\eta}}{\partial s_j} \right\}^T \quad (117)$$

The third terms in Equation 110 are

$$I_{\Gamma_{3i}}^P = -\int_P \tilde{a} g N_i^P ds = -\tilde{a} g \int_P N_i^P ds = -\frac{1}{2} \tilde{a} g L^P = I_{\Gamma_{3j}}^P$$

therefore,

$$[I_{\Gamma_3}^P] = [\Gamma_3^P] = -\frac{1}{2} \tilde{\alpha} \mathbf{gL}^P \begin{pmatrix} 1 \\ 1 \end{pmatrix} \quad (118)$$

The function  $\hat{\eta}$  will be obtained by first computing the element matrix  $[A^e]$  and  $[B^e]$  for elements  $e = 1, \dots, E$ , and the boundary matrix  $[C^P]$ ,  $[\Gamma_1^P]$ ,  $[\Gamma_2^P]$ ,  $[\Gamma_3^P]$  for segments  $P = 1, \dots, N^P$ . These matrices are assembled to obtain an  $N \times N$  system of equations,

$$\sum_{\Omega} ([A^e] + [B^e]) \{\hat{\eta}^e\} + \sum_C [C^P] \{\hat{\eta}_C^P\} + \sum_{\Gamma} ([\Gamma_1^P] + [\Gamma_2^P]) \{\hat{\eta}_\Gamma^P\} + \sum_{\Gamma} [D^P] + \sum_{\Gamma} [\Gamma_3^P] = 0$$

Notice that

$$\sum_{\Gamma} [D^P] = -\tilde{\alpha} \mathbf{qr}^2 \left\{ \frac{\partial \hat{\eta}}{\partial s} \Big|_{A_1}, -\frac{\partial \hat{\eta}}{\partial s} \Big|_{A_2} \right\}^T = \alpha \tilde{\alpha} \mathbf{qr}^2 \begin{bmatrix} 1 & 0 \\ 0 & 1 \end{bmatrix} \{\hat{\eta}_{A_1}, \hat{\eta}_{A_2}\}^T \quad (119)$$

where  $A_1$  and  $A_2$  are two points that connect the open boundary and coastal boundary and the wall boundary condition, (9), applies to  $\partial \hat{\eta} / \partial s$ . Therefore, term  $\sum_{\Gamma} [D^P]$  can be included into  $\sum_C [C^P] \{\hat{\eta}_C^P\}$  and then the assembled equation becomes

$$[K_1] \{\hat{\eta}\} + [K_2] \{\hat{\eta}_C\} + [K_3] \{\hat{\eta}_\Gamma\} = \{f\} \quad (120)$$

or

$$[A] \{\hat{\eta}\} = \{f\} \quad (121)$$

This linear system of equations may be solved to obtain  $\eta$ .

## 4.4 Kinematic Parameters

Once a solution for  $\hat{\eta}$  is obtained in CGWAVE, the maximum wave velocity, maximum wave pressures, wave phase angle and wave amplitude may be obtained from the values of  $\hat{\eta}$ . These quantities are obtained as follows.

The velocity potential for water particles of surface water waves may be written as

$$\Phi(x, y, z, t) = [\phi_1 \cos \omega t + \phi_2 \sin \omega t] Z(z) \quad (122)$$

where

$$Z(z) = \frac{\cosh[k(z+h)]}{\cosh(kh)} \quad (123)$$

The potential may be expressed in terms of  $\hat{\eta}$  by substituting

$$\Phi = \frac{g}{i\omega} \hat{\eta} \quad (124)$$

into Equation 122; this gives

$$\Phi(x, y, z, t) = \frac{g}{\omega} \Re \left[ \hat{\eta}(x, y) e^{-i\left(\frac{\pi}{2} + \omega t\right)} \right] Z(z) \quad (125)$$

where

$$\hat{\eta} = \hat{\eta}_1 + i\hat{\eta}_2 \quad (126)$$

This expression may be written as follows by separating the real,  $\hat{\eta}_1$ , and imaginary,  $\hat{\eta}_2$  parts on  $\hat{\eta}$ , and replacing  $-\pi/2-\omega t$  with  $\alpha$ ; this gives

$$\Phi = \frac{g}{\omega} [\eta_1 \cos \alpha + \eta_2 \sin \alpha] Z \quad (127)$$

An expression for the velocity of water particles is obtained by evaluating the gradient of the expression for  $\Phi$  in the last equation; this gives

$$v_x = \frac{g}{w} \left[ \left( \frac{\partial \hat{\eta}_1}{\partial x} \right) \cos \alpha + \left( \frac{\partial \hat{\eta}_2}{\partial x} \right) \sin \alpha \right] Z \quad (128a)$$

$$v_y = \frac{g}{w} \left[ \left( \frac{\partial \hat{\eta}_1}{\partial y} \right) \cos \alpha + \left( \frac{\partial \hat{\eta}_2}{\partial y} \right) \sin \alpha \right] Z \quad (128b)$$

These expressions contain the horizontal components of the velocity. For simplicity,  $Z$  is taken as a local constant.

The magnitude of the horizontal components of the velocity is obtained by substituting  $v_x$  and  $v_y$  from the last expression into

$$|v|^2 = (v_x)^2 + (v_y)^2 \quad (129)$$

to obtain

$$|v|^2 = \left( \frac{g}{\omega} \right)^2 Z^2 \left\{ \left[ \left( \frac{\partial \hat{\eta}_1}{\partial x} \right)^2 + \left( \frac{\partial \hat{\eta}_1}{\partial y} \right)^2 \right] \cos^2 \alpha + \left[ \left( \frac{\partial \hat{\eta}_2}{\partial x} \right)^2 + \left( \frac{\partial \hat{\eta}_2}{\partial y} \right)^2 \right] \sin^2 \alpha - \left[ \frac{\partial \hat{\eta}_1}{\partial x} \frac{\partial \hat{\eta}_2}{\partial x} + \frac{\partial \hat{\eta}_1}{\partial y} \frac{\partial \hat{\eta}_2}{\partial y} \right] \sin(2\alpha) \right\} \quad (130)$$

The maximum horizontal velocity occurs at locations where the derivative of  $|v|^2$  with respect to  $\alpha$  is equal to zero; this occurs where

$$\left\{ - \left[ \left( \frac{\partial \hat{\eta}_1}{\partial x} \right)^2 + \left( \frac{\partial \hat{\eta}_1}{\partial y} \right)^2 \right] + \left[ \left( \frac{\partial \hat{\eta}_2}{\partial x} \right)^2 + \left( \frac{\partial \hat{\eta}_2}{\partial y} \right)^2 \right] \right\} \sin(2\alpha) - 2 \left[ \frac{\partial \hat{\eta}_1}{\partial x} \frac{\partial \hat{\eta}_2}{\partial x} + \frac{\partial \hat{\eta}_1}{\partial y} \frac{\partial \hat{\eta}_2}{\partial y} \right] \cos(2\alpha) = 0 \quad (131)$$

Rearranging terms gives

$$\alpha = \frac{1}{2} \arctan \left[ \frac{2 \left[ \frac{\partial \hat{\eta}_1}{\partial x} \frac{\partial \hat{\eta}_2}{\partial x} + \frac{\partial \hat{\eta}_1}{\partial y} \frac{\partial \hat{\eta}_2}{\partial y} \right]}{- \left[ \left( \frac{\partial \hat{\eta}_1}{\partial x} \right)^2 + \left( \frac{\partial \hat{\eta}_1}{\partial y} \right)^2 \right] + \left[ \left( \frac{\partial \hat{\eta}_2}{\partial x} \right)^2 + \left( \frac{\partial \hat{\eta}_2}{\partial y} \right)^2 \right]} \right] \quad (132)$$

The magnitude of the horizontal component of the velocity will have its minimum and maximum values at this value of  $\alpha$  and at  $\alpha + \pi/2$ . The value of  $|v|$  is calculated at both of these angles; the larger value is the maximum velocity over all times.

The pressure is obtained from the linear form of the Bernoulli equation;

$$\frac{\partial \Phi}{\partial t} + \frac{P}{\rho} + gz = \text{constant} \quad (133)$$

Note that the pressures associated with velocities (dynamic head,  $\frac{1}{2}v^2$ ) are ignored in this linear form. The expression for  $\Phi$  in Equation 125 is substituted into this expression and terms are rearranged to obtain

$$P = -\rho gz + \rho g \Re(\hat{\eta} e^{-i\omega t}) Z + \text{constant} \quad (134)$$

The maximum pressure over a wave cycle occurs when the term  $\Re(\hat{\eta} e^{-i\omega t})$  is equal to  $H/2$ . The constant is chosen such that the hydrostatic pressure is equal to zero at  $z=0$ ; thus

$$P_{\max} = -\rho g z + \rho g \frac{H}{2} Z \quad (135)$$

The wave phase angle  $\beta$  is obtained from

$$\beta = \arctan \frac{\hat{\eta}_2}{\hat{\eta}_1} \quad (136)$$

The cosine of  $\beta$  varies from -1 to 1, and is written as output.

The wave amplitude  $A$  is obtained from

$$A = \sqrt{\hat{\eta}_1^2 + \hat{\eta}_2^2} \quad (137)$$

A ‘snap-shot’ of the sea surface elevation at time = 0.0 is obtained from

$$\eta = \Re[\hat{\eta} e^{-i\omega t}] = [\hat{\eta}_1 \cos \omega t + \hat{\eta}_2 \sin \omega t] \quad (138)$$

## 4.5 Floating Docks

A floating dock inside the computational domain may be treated following the formulation of Tsay & Liu (1983). If the distance from the bottom of the bed to the surface of the floating body is  $\bar{d}(x, y)$  and the wave number corresponding to this depth is  $\bar{k}(x, y)$ , the governing equation for region under the floating body is

$$\nabla \cdot (p \nabla \hat{\eta}) = 0 \quad (139)$$

where

$$p = \frac{1}{2} \left( \frac{\sigma}{\bar{k}} \right)^2 \left( 1 + \frac{2\bar{k}\bar{d}}{\sinh 2\bar{k}\bar{d}} \right) \quad (140)$$

$$\sigma^2 = g\bar{k} \tanh \bar{k}\bar{d} \quad (141)$$

Note that the second term of Equation 1 has been neglected in Equation 139. This

simplification is known as the ‘rigid lid’ approximation. Tsay and Liu (1983) have demonstrated that this formulation gives very good results when compared with some exact solutions. Equation 139 is solved in CGWAVE in place of Equation 1 for the region where a floating structure is present in the domain  $\Omega$ .

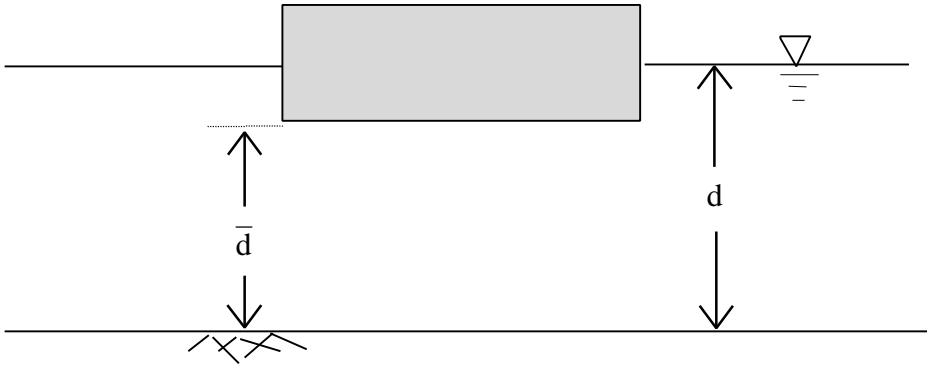


Figure 6. Definition sketch for floating structures

# 5 ITERATIVE CG SOLUTION METHOD

CGWAVE provides the choice of choosing the wavelength dependent resolution to solve the governing equation. An in-depth investigation was performed to determine the sensitivity of the solution as a function of wavelength. Based on our analysis, it is recommended that ten or more points per wavelength to be used. In regions where the change in topography or wave-amplitude is rapid, a finer grid is necessary. To solve the elliptic mild-slope equation without approximating the physics (as in parabolic models), the problem has to be solved simultaneously over the entire domain. This leads to a very large linear system of equations (e.g. Equation 69). Direct methods (e.g. Gaussian elimination) are often inapplicable due to extremely large storage requirement of the matrix  $[A]$ . Iterative methods, on the other hand, require memory for only the non-zero elements in  $[A]$ . Since  $[A]$  is highly sparse, iterative methods can significantly enhance the ability of the elliptic type mild-slope equation models to handle large domain problems. However, most iterative procedures require  $[A]$  to be diagonally-dominant or symmetric and positive-definite. Unfortunately, the coefficient matrix  $[A]$  is not diagonally-dominant, nor symmetric and positive definite. Panchang et al. (1991) recommended that the following Gauss transformation is applied to Equation 69 :

$$[A^*][A]\{\hat{\eta}\} = [A^*]\{f\} \quad (142)$$

where  $A^*$  is the complex conjugate transpose of  $[A]$ . Xu (1995) has shown that the new coefficient matrix  $[A^*][A]$  is Hermitian and positive-definite. Therefore, the modified conjugate-gradient method, which is often several orders of magnitude faster than many other schemes, including the traditional conjugate gradient scheme, is guaranteed to converge when applied to Equation 125. The algorithm is implemented in CGWAVE as

follows:

1. Select trial values for  $\{\hat{\eta}_0\}$  (i.e. 0<sup>th</sup> iteration) for all nodes in model domain where the solution is desired.
2. Compute for all points the residual  $\{r_0\} = \{f\} - [A] \{\hat{\eta}_0\}$  and the left hand side of Equation 125 as  $\{p_0\} = [A^*] \{r_0\}$ .
3. Compute for the i<sup>th</sup> iteration the parameters  $\alpha_i$ , defined as:  $\alpha_i = \frac{\|[A^*] \{r_i\}\|^2}{\|[A] \{p_i\}\|^2}$
4. Update  $\{\hat{\eta}_{i+1}\} = \{\hat{\eta}_i\} + \alpha_i \{p_i\}$  for all points.
5. Check for convergence of the solution. The criterion for convergence used in CGWAVE is

$$\frac{\|[A] \{\hat{\eta}_{i+1}\} - \{f\}\|^2}{\|\{\hat{\eta}_{i+1}\}\|^2} < \varepsilon \quad (143)$$

where  $\varepsilon$  is a prescribed tolerance. If Equation 126 is satisfied, stop.

6. If Equation 126 is not satisfied, compute, for each grid point,  $\{r_{i+1}\} = \{r_i\} - \alpha_i [A] \{p_i\}$ .
7. Compute for the i<sup>th</sup> iteration:  $\beta_i = \frac{\|[A^*] \{r_{i+1}\}\|^2}{\|[A^*] \{r_i\}\|^2}$ .
8. Compute  $\{p_{i+1}\} = [A^*] \{r_{i+1}\} + \beta_i \{p_i\}$ .
9. Set  $i = i + 1$ , and go to step 3.

In the procedure above, the module of an array  $\|\{x\}\|$  is defined as

$$\|\{x\}\| = \left( \sum_{i=1}^N |x_i|^2 \right)^{1/2} \quad (144)$$

This procedure has been demonstrated to work very well in finite-element models. In fact, these techniques were found to be far more efficient in the present finite-element runs than for the finite-difference studies of Xu & Panchang (1993) and Panchang et al. (1991).

Li (1994) has recently suggested modifications to the iterative schemes of Panchang et al. (1991) for enhancing the convergence. Comparison between these two schemes were given in Xu and Panchang (1995). Although these modifications resulted in faster convergence, it was noticed that, unlike the basic procedures of Panchang et al. (1991), they do not converge to a solution monotonically. Instead, the residual error decreases in an oscillatory manner as the iterations proceed. Also, the gain in CPU time varies from case to case and appears to be problem-specific, but it can save over 50% of CPU time for some applications. This scheme has also been included in CGWAVE as an alternative choice, and consequently, there are two types of solvers provided in CGWAVE.

The solving algorithm is slightly different when non-linear mechanisms are incorporated into the solution. In this case, the solution is first solved as if there were no non-linear mechanisms. This solution is then used to prescribe initial conditions for the non-linear mechanisms, and the system of equations are modified to incorporate the resulting non-linear mechanisms. CGWAVE then solves using the modified equations. This iterative method of solving, modifying the system of equations with non-linear mechanisms, and solving again continues until the resulting solution no longer changes between iterations.

The solving algorithm is also different when spectral wave conditions are used. In this case, a solution is first obtained for each individual spectral component. The final solution is obtained by linear superposition of the solutions for all spectral components. This superposition is performed after a spectral run is completed, using a post processing program.

# 6 GENERATION OF FINITE-ELEMENT NETWORK

CGWAVE requires a two-dimensional (2D) triangular grid network for its finite-element calculations. Although several grid generation packages are available, they are not suitable for elliptic coastal wave models for which the size of the elements must be related to the wave length (which varies with local water depth) for proper resolution. A semicircular open boundary has to be created for special open boundary treatment, and reflection coefficients, which may vary from one part of the coastal boundary to another, are also required as input data for the model. To deal with these special problems, CGWAVE has been interfaced with the grid-generator associated with the SMS (Surface water Modeling Systems) flow modeling package. The Engineering Computer Graphics Laboratory is developing this state-of-the-art package for the US Army Corps of Engineers at Brigham Young University.

SMS contains a set of 2D hydrodynamic models and a general purpose grid generation and visualization package. SMS includes an efficient finite-element grid-generator. However, this grid-generator was originally designed for other types of hydrodynamic models. Three utility programs that help interface CGWAVE with the SMS grid-generator have been developed for use outside SMS, prior to the full integration of CGWAVE into SMS. Given a coarse rectangular array of bathymetric data, these programs generate a wavelength-dependent triangular nodal network (based on the user-specified resolution, i.e. the number of points per wave length), automatically construct the semi-circular open boundary, assign reflection coefficients along the coastal boundaries, eliminate unwanted land points, etc. The resulting grid and boundary data from SMS are then filtered by another utility program for use by the wave model. The output from the wave model can be processed and then plotted by using SMS. This makes model implementation very efficient and allows the user to view a graphic representation of the solution.

# 7 PROCEDURE FOR STAND-ALONE USAGE OF CGWAVE

CGWAVE is an efficient and easy-to-use wave model. Although more advanced features are anticipated to evolve in the future, the current version is sufficiently user-friendly and can provide the base information for shallow water wave propagation and transformation for harbor/coastal problems or offshore open sea problems. The information provided by this model can be further used to calculate wave forces on structures, stability of breakwaters, sediment/pollutant transport and can be used to assist harbor/coastal protection structure design.

In this section of the manual, step-by-step instructions are given for use of CGWAVE. The procedure outlined here pertains to the usage of CGWAVE as stand-alone (i.e. outside SMS); this usage is referred to as MODE-1. MODE-1 usage does require the use of SMS for some procedures. A similar, automated procedure is available within SMS, and is referred to as MODE-2. After successful installation of CGWAVE and SMS, the user can proceed with applications of CGWAVE. In general, the MODE-1 application of CGWAVE consists of eight steps:

**Step 1.** After a region for simulation has been chosen, a file containing (x,y,z where z = depth) data in rectangular fashion may be created from a map or other data base. The input file format is described in detail in section 7.2.2 of this manual and in the File Formats section of the SMS Reference Manual.

**Step 2.** The raw data gathered in Step 1 is processed by the program “resol”. Coastal and open boundaries are defined and most extraneous data is eliminated. Wavelength dependent resolution is established, and the revised (x,y,z) data set is presented for constructing the finite element grid.

**Step 3.** The finite element grid is constructed using SMS, and boundary conditions are assigned to the open and coastal boundaries.

**Step 4.** CGWAVE input parameters are specified. These parameters include: incident wave condition, nonlinear mechanisms (wave breaking, bottom friction and nonlinear dispersion), choice of solvers, choice of open boundary condition, iteration control parameters, etc.

**Step 5.** All relative information needed for input to the model is consolidated into a single input file. This processing is done by program “reform”.

**Step 6.** Run the wave model and obtain an output wave potential file.

**Step 7.** Process the output file (using program “trans”) to obtain amplitude, phase and kinematics solution files.

**Step 8.** Use SMS to view various solution images using a variety of contouring options.

## 7.1 File Descriptions

The following files contain source code for the CGWAVE modeling package:

cgwave.f	-- Fortran source code of CGWAVE.
cgwave.gen	-- Template of the general information file.
reform.f	-- Fortran source code of reform.
resol.f	-- Fortran source code of resol.
trans.f	-- Fortran source code of trans.

Given below is a list of example files for application of CGWAVE. Although one can use any name for them, the following convention is used throughout this manual. It is also recommended that the user follow this convention for simplicity and consistency.

filename.xyz	-- File to be imported to SMS and to be used by program “resol”. Contains (x,y,depth) data describing the bathymetry.
filename.bc	-- Boundary condition file created by SMS.
filename.geo	-- Geometry file created by SMS.

- filename.gen -- General information file, text format. Contains required input control parameters for CGWAVE.
- filename.dat -- CGWAVE and “trans” input data file. Created by program “reform”.
- filename.out -- CGWAVE wave potential output file. Input to program “trans”
- filename.txt -- Text output file created by trans. Contains general information about the project modeled, CGWAVE input parameters, solution status and complete output of x,y depth, amplitude and phase at each node in text format.
- filename.sol -- Solution output file created by program “trans”. Contains information about computed amplitude, phase and kinematics. May be read by SMS for graphic presentation of the solution. ASCII text format.
- filename.pls -- User created input file for program “trans” which provides information about selected node ids, points, lines and rectangular sub-regions where output is desired.
- filename.sel -- Selected locations output file created by program “trans”.
- filename.flw -- Floating dock solution output created by program “trans”. Of relevance only if there is a floating dock inside the computational domain. Velocity potential output is available in this sub-domain, which may be further used (outside CGWAVE) to calculate forces and moments.
- filename.alp -- Animated film loop for view of variations in amplitude and phase with time. For use in SMS.

## **7.2 Raw Data Processing – Program “resol”**

Grid resolution is dependent on the local water depth. In general, 10 or more nodes per (local) wavelength are desired. In most cases, a large number of extra nodal points must be created over the raw data points to satisfy the resolution requirements. Hence it is desirable to have these points generated before using SMS to create a finite

element network. Nodes with negative or zero depths (dry land) are prohibited within the computational domain. A minimum water depth may be judiciously chosen and regions under this minimum depth (higher in elevation) should be eliminated. For the open boundary, it is necessary to have properly distributed points created on a semicircle (or full circle for offshore applications), and points outside the open boundary must be discarded. These tasks are theoretically trivial, but very time consuming. The utility program “resol” accomplishes these tasks quickly and with minimal effort on the part of the user.

## **7.2.1 Viewing XYZ Data and Selecting Open Boundary End Points**

Consider as an example the raw data-set called “swansr.xyz”. This raw data may be viewed in SMS. This can be done as follows. Run the SMS executable file. When SMS is open, a tool palette, graphics window, and pull-down menus at the top of the screen are visible. From the “File” menu choose “import”. Select “XYZ data” from the “Select Import Format” window. Select the drive, directory and file “swansr.xyz” using the “Open” window. From the tool palette select the “Create Linear Triangle” tool. Note that the name of the tool that is currently under the mouse pointer is displayed at the bottom of the SMS window. From the “Elements” menu select “Triangulate”. This results in a finite element triangular network. Select the “Display Options” tool from either the tool palette or from the “Display” pull-down menu. The “Display Options” window allows the user to view or hide various display features. Toggle off “Nodes”. Toggle the “Contours” on. Click on the “Options” button to the right of the “Contours” toggle. Select “Color fill between contours”, click “OK”. Click “OK” again to exit the “Display Options” window. A color representation of the triangulated grid is now visible. It is suggested that the user become familiar with the function of the tools and options before attempting any serious modeling effort. Before exiting SMS, the user should write down some information that is used to create the semicircular open boundary. Pick a minimum water depth and roughly estimate the starting and end point

coordinates (counter-clockwise) of the semicircular open boundary. Since the wave model does not allow zero or negative depths in the computational domain, a minimum depth must be specified when executing the program “reso!”. Make sure that both semicircle end points are inside an area where water depth is greater than the minimum depth on at least one node of the background “rectangle”. In this example, 2.0 (meters) is used as the minimum depth and the points (3500.0,2700.0),(100.0,2450.0) as the starting and end point coordinates for the semicircle. You may now quit the SMS (do not save any file information at this time).

## 7.2.2 XYZ File Format

The input data file for the program “reso!” must be a rectangular domain with constant dx and dy for each direction. The file has the following format:

```
XYZ
x1 y1 z1
x2 y2 z2
.
.
.
xn yn zn
```

For example, by viewing “swansr.xyz” with a text editor, the following will be seen:

```
XYZ
0.0 0.0 0.0
0.0 200.0 0.0
0.0 400.0 0.0
0.0 600.0 0.0
0.0 800.0 0.0
0.0 1000.0 0.0
0.0 1200.0 0.0
0.0 1400.0 0.0
0.0 1600.0 0.0
0.0 1800.0 0.0
0.0 2000.0 0.0
0.0 2200.0 0.0
```

```

0.0 2400.0 0.0
0.0 2600.0 15.3
0.0 2800.0 15.3
0.0 3000.0 15.3
0.0 3200.0 14.9
0.0 3400.0 23.8
0.0 3600.0 23.8
0.0 3800.0 27.5
0.0 4000.0 15.3
0.0 4200.0 24.4
0.0 4400.0 13.7
200.0 0.0 0.0
200.0 200.0 0.0
200.0 400.0 0.0

```

Note that this is only the top portion of the swansr.xyz file. The first line must be “XYZ” followed by (x y z) data. This xyz file should be oriented such that the x-axis points to the east on the screen when the data set is displayed.

### 7.2.3 Program “resol”

Execution of program “resol” will result in the creation of a new XYZ data file called “swanst.xyz”, which is to be used as input to SMS for further grid generation operations. This file has better resolution than the raw data file (e.g. swansr.xyz), and contains information regarding the semicircular open boundary.

To begin the example, run the “resol” executable. A program information header will be displayed on the screen. The following information will appear after the header:

```

Input filename : (*.xyz)
swansr.xyz      (Hit <Enter> after each response)

```

```

Output Filename: (*.xyz)
swanst.xyz

```

```

Input data spacing.
Dx is:
200.0

```

```

Dy is:

```

200.0

Incident wave period

30.0

Enter type of open boundary:

Full Circle (=0), Semi Circle (=1)

1

Start from:

3500.0 2700.0

End at (ccw):

100.0 2450.0

Are they Fixed (=0) or Approximate (=1) ?

1

Number of Nodes per Wavelength :

10

Interpolate between land and water ?

(yes=0, no=1)

0

Minimum Water Depth :

2.0

Minimum Node Spacing :

.001

Starting point of the semicircle :

3511.111 2711.111

End point of the semicircle :

80.000 2440.000

End of program, Press Enter to continue

Some notes regarding the above questions and answers follow.

**Minimum Water Depth.** When specifying a minimum water depth, the estimated semicircle end points may or may not satisfy the minimum depth criteria. In most cases,

these coordinates will be either inside or outside the domain (and rarely on the exact boundary indicated by the minimum depth.) By choosing “Approximate”, the program “resol” will locate a boundary point closest to the point specified. Note also that program “resol” requires that the location of the estimated points should lie inside a rectangle (of the background or raw data network) with at least one corner having a depth greater than or equal to the minimum depth.

**Number of Nodes per Wavelength.** It is strongly recommended that at least 10 or more points per wavelength be used whenever possible. A resolution of 7 or 8 points per wavelength may yield a reasonable solution, but 6 should be treated as an absolute minimum. 15 points per wavelength are sufficient for most applications.

**Interpolate Between Land and Water.** Other than some ideal cases with constant depth (e.g. laboratory or analytical test cases), always answer yes to this question.

**Minimum Node Spacing.** This feature allows the user to limit the density of nodes (and, indirectly, the total number of nodes) placed within the domain. This may be necessary for extremely shallow regions or for very large domains. This feature can contradict the “Number of Nodes per Wavelength” parameter, and should be used with caution. It is recommended that the user set this parameter to a very small value (.001 or smaller) for most applications.

## 7.3 Creation of Finite Element Grid

A description of the steps involved in creating a finite element grid and constructing CGWAVE input files using SMS follows. This procedure describes MODE-1 usage of CGWAVE. It is highly recommended that the user be fully familiar with the MODE-1 usage, since the automated procedure for MODE-2 makes use of the steps described below. In MODE-1, the user needs to create the following files:

\*.geo           (geometry file)

- \*.bc (boundary condition file)
- \*.gen (general input file)

These files are used by the program “reform” to construct the main CGWAVE input data file. Specific steps pertinent to creating each of the above files are provided below.

### 7.3.1 Geometry

Open SMS. From the “File” menu choose “import”. Select “XYZ data” from the “Select Import Format” window. Select the drive, directory and file “swanst.xyz” in the “Open” window. From the tool palette select the “Create Linear Triangle” tool. From the “Elements” menu select “Triangulate”. Any nodes and elements that lie outside the desired model domain must be manually removed. Using the “Select Element” and “Select Nodes” tools does this. The <Shift> and <Ctrl> keys may be used in combination with these tools to remove multiple and groups of elements or nodes. For example, a group of elements may be selected for deletion as follows: Hold the <Ctrl> key, click (do not release) the mouse button on the center of an element. Drag the pointer across the group of elements to be deleted. An arrow beginning at the first selection point should follow the pointer. Any element touched by this arrow will be selected. Elements may be added to (or removed from) a selection group by holding the <Shift> key while selecting an element. The selected elements are then deleted with the <Del> key. Other selection methods are available in the “Edit” and “Elements” menus. Remember to clean up and/or remove the elements in areas where islands or structures are located. After obtaining a satisfactory grid-network, boundary conditions must be specified, as detailed in the following section. Select “Save Geometry” in the “RMA2” menu. Name the file swanst.geo.

### 7.3.2 Boundary Conditions

**Defining Open and Coastal Boundaries.** The boundary conditions for this grid may now be specified. Pick “Create Nodestring” tool from the tool palette. This tool is used to identify the nodes along the edge of the model domain. Use the mouse pointer to select the start point (node) of the semicircular open boundary. (The “Zoom” tool may be used to help identify the start node.) Press and hold the <Ctrl> key and select the end point (node) of the semicircular open boundary. Press <Enter>. The open boundary has been defined by a single “nodestring”. For open sea/offshore problems, where open boundary is a full circle, similar procedure applies. For this example, we will next define the coastline boundary using a single string. Proceed with the above selection procedure, this time using the end point of the semicircle as the new start point. The new end point is the start point of the semicircle. In some modeling situations, the user may want to assign different reflection coefficients to sections of the coastline. If this is the case, a nodestring must be created for each area of differing reflection coefficient. A new nodestring must always begin with the end point of the previous string. The direction of nodestrings should be specified such that when moving from the start point to the end point of the nodestring, the modeled domain is on the left side of the nodestring, i.e. counter-clockwise.

**Defining Islands Boundaries.** Island boundaries are defined in much the same way as described above, with the following exceptions. Island nodestrings are created such that the modeled domain is on the right side of the nodestring when moving from the start point to the end point, i.e. counter-clockwise. A complete island boundary must consist of two or more nodestrings, as SMS does not allow a single nodestring to begin and end on the same node. Islands should be defined after all open and coastal boundaries have been defined.

**Assigning Reflection Coefficients.** Pick “Select Nodestring” tool. A small selection area (box) should appear in the center of each nodestring. Place the pointer on the selection box for the open boundary and select it. Go to the “RMA2” menu and select

“Assign BC...”. In the “RMA2 Assign Boundary Condition” window, pick the ‘Head BC’ option. Set the elevation (lower part of the window) to 5.0. This value is used to tell CGWAVE that this nodestring is an open boundary. Click “OK”. Repeat this procedure for all other boundaries. For all boundaries other than the open boundary, the elevation value represents the reflection coefficient and should be between 0.0 and 1.0, corresponding to the reflection coefficient of that portion of coastal boundary (including islands). The value of 1.0 for reflection coefficient should be used for a fully reflecting boundary and 0.0 used for fully absorbing boundary. Save the boundary condition information by selecting “Save BC...” from the “RMA2” menu. For the example case, name the file “swanst.bc”.

**Floating Structures.** Floating structures are discussed in detail in section 4.5. When a floating structure is included inside the domain, the elements containing the floating structure must be both marked and adjusted to signify and account for the presence of the structure. The elements contained by the area of the floating structure are assigned a “Material Type ID” of “3” as follows. First, select all the elements within an area bounded by the perimeter of the floating structure. Then select “Assign Material Type” from the “Elements” menu. Click on the “New” button in the “Materials Editor” until the “ID:” changes to “3”. Click “Select”. Next, modify the depth of the nodes in this area as described in section 4.5. The new depths are shown in Figure 6 as  $\bar{d}$ . This can be done using the “Transform Mesh” option found in the “Nodes” menu. CGWAVE will now recognize this area as a floating structure and treat it accordingly.

**Renumbering the Geometry.** After completing the grid generation and boundary definition, the grid must be renumbered. Using the “Select nodestring” tool, select any of the nodestrings. From the “Elements” menu choose “Renumber”. In the “Renumbering Opts” window, select “Band Width” and then “OK”. After renumbering, the grid generation process is complete. Re-save the geometry and boundary condition files using the same names given before (swanst.geo and swanst.bc). Some basic information about

the grid may be viewed by clicking the “Display Module Info” tool, or by selecting “Get Info...” from the “File” menu. You may now quit SMS.

## 7.4 The General Information File (\*.gen)

A template called “cgwave.gen” is provided for the benefit of the user. A new copy of this file should be made for each application. The contents of the file are written in ASCII text and appear below. Note that the incident wave conditions contain data for a single (monochromatic) model run. Spectral input conditions may be input by including additional lines below the first (Angle/Period/Amplitude) line. Two empty (blank) lines should follow the last (Angle/Period/Amplitude) line, separating it from the “2) Open Boundary ...” line. Incident angles are measured in degrees and the incident direction is defined such that the incident wave travels in the positive x-direction when  $\theta_i$  is equal to zero.

PROJECT : Project Name

(...blank line)

(...blank line)

1) Incident Wave Conditions:

(...blank line)

No. Incident Wave Angle || Wave Period (s) || Incident Wave Amplitude

1	0.0	30.0	1.0
---	-----	------	-----

(...blank line)

(...blank line)

2) Open Boundary (Bessel Series = 0, Parabolic = 1, Box = 2) : 1

(...blank line)

If Bessel Series, Number of Terms Used : 50

If Parabolic, Exterior Coastline Reflection : 0.0

(...blank line)

(...blank line)

3) Bottom Friction (Yes=1,No=0) ? 0

(...blank line)

If Yes, Friction Coefficient : 0.12

(...blank line)

(...blank line)

4) Wave Breaking (Yes=1,No=0) ? 0

(...blank line)

If Yes, Breaking Coefficient : 0.15

(...blank line)

(...blank line)

5) Nonlinear Dispersion Relation (Yes=1,No=0) ? 0

(...blank line)

(...blank line)

6) Solver (cg standard == 0, modification == 1) : 1

(...blank line)

Tolerance of Convergence for Linear Equations : 0.1E-8

Interval for Checking Convergence : 100

Maximum Iterations for the Linear Equations : 100000

(...blank line)

(...blank line)

7) Tolerance of Convergence for Nonlinear Mechanisms : 0.0001

(...blank line)

Maximum Iterations for the Nonlinear Mechanisms : 8

(...blank line)

(...blank line)

end of data

This file provides the basic incident wave and boundary type information and various control parameters for CGWAVE. Due to the programming methods used to read the data from this file, the text must not be altered. The parameter values may be replaced

with values that are specific for the new application. All the numbers must be present and in the correct location, whether they are used or not.

## 7.5 Assembly of Input Information - Program “reform”

The program “reform” is used for assembling and converting all input information into the format needed by CGWAVE. It reads the geometry, boundary condition and general information files and constructs a unified input data file for CGWAVE. The program also verifies some components of the provided data. Program “reform” makes the central part of CGWAVE portable. In other words, a workstation may be used to create and manipulate the graphics, and CGWAVE may be run on any other platform (PC, mainframe, etc.). Also, because “reform” sorts and rewrites the data in clean, nested groups, the same data set can be used to perform simulations with different incident wave directions, different combinations of boundary reflection coefficients, different incident wave amplitudes and periods (to some extent, since resolution is wave period dependent), etc. without going through the trouble of editing the general information file and re-running “reform” for each case. This is done by simply editing a few lines in the top sections of the data (\*.dat) file. Another feature of “reform” that is especially useful is the ability to check the grid resolution for the overall domain.

Here, the rectangular harbor test is used to demonstrate of the function of “reform”. Run the program “reform”. After the informational header, the following appears on the screen:

```
General information filename: (*.gen)
rect.gen
```

```
Boundary condition filename from SMS: (*.bc)
rect.bc
```

```
Geometry filename from SMS: (*.geo)
rect.geo
```

```
Output data filename for CGWAVE: (*.dat)
rect.dat
```

Do you want resolution analysis (yes/no) ?  
yes

Number of points per wave length distribution (%)

From 0 to 5 : .0

From 5 to 6 : .0

From 6 to 7 : .0

From 7 to 8 : .0

From 8 to 9 : .0

From 9 to 10: .0

From 10 to 11: .0

From 11 to 12: .0

From 12 to 13: .0

From 13 to 14: .0

From 14 to 15: .0

From 15 up : 100.0

End of program, Press ENTER to continue

The last set of information following “Number of points per wave length distribution (%)” is the resolution data for this geometry, calculated from the grid-network and wave period specified by the user in the general information file. As stated earlier, less than 5 grid points per wavelength is not valid, over 15 points per wavelength is generally very good. The resolution data shown is for the entire computational domain and it gives the resolution distribution for all the elements. This information is output to the screen only. The user may copy and retain it manually for later reference. This feature is also useful if the same grid is to be used again with a different wave period; the resolution analysis will help to determine whether or not grid modification is necessary. This may be the case if the new wave period is smaller than the original design period wave.

## 7.6 The Wave Model - Program “cgwave”

This is the main part of the CGWAVE model. When program “cgwave” is run for the rectangular harbor case, the following prompts appear:

```
Input data filename: (*.dat)
rect.dat
```

```
Output wave potential filename: (*.out)
rect.out
```

A block of information reviewing input parameters is printed to the screen. This is followed by messages regarding the processing of input information. A “hot start” (or re-start) option then follows:

```
A previous solution file as initial state (y/n) ?
n
```

```
Iterations Begin, Please Wait .....
```

The model will run until either the convergence parameter or the maximum number of iterations parameter is met or exceeded. The solution will then be written to the file (\*.out) specified earlier. The “hot start” option allows the user to restart the model with computations beginning from an old CGWAVE output file. This can be useful in the event that the model is forced to write a solution (\*.out) before the convergence criteria have been reached. This “partially converged” solution will occur if the “Maximum Iterations for the Linear Equations” parameter is exceeded before the “Tolerance for Convergence of Linear Equations” parameter is reached.

## 7.7 Post-processing the Output - Program “trans”

The output from program “cgwave” is a file (e.g. rect.out) which contains grid information and calculated complex wave elevations. The program “trans” may be used to convert these potentials into a readily usable format or to obtain output at desired locations.

### 7.7.1 Program “trans”.

Reformed data filename (used as input to CGWAVE) : (\*.dat)

rect.dat

Wave potential file (output from cgwave): (\*.out)

rect.out

Please select one for output:

g General info only

t General info with complete text output

n None above

The “General info only” option prints text information about the input parameters and number of iterations required to obtain the solution. The “General info with complete text output” option adds the node numbers, location, computed wave amplitude and phase information to the general information output. The naming convention used for the file is “filename.txt”.

Create output of amplitude and phase for SMS (yes/no) ?

This output provides information in a format that is readable by SMS and is used for graphic viewing of amplitude, phase and sea surface elevation at time = 0. The naming convention is “filename.sol”. This convention deviates from the SMS \*.sol file naming convention in that the CGWAVE \*.sol files are written in ASCII text format.

Create output of water particle kinematics (yes/no) ?

This output provides maximum horizontal velocities and pressure gradients. The naming convention is “filename-kin.sol”.

Create time series output file for velocity  
and surface elevation animation (yes/no) ?

An animated view of the velocity and surface elevation can be created for viewing in SMS. The file naming convention is “filename.alp”.

Do you want output at selected locations (yes/no) ?

Amplitude and phase data can be extracted at discrete output points or along lines (transects) or in rectangular sub-regions. The coordinates of the points, lines and sub-regions may be specified directly from the keyboard or read from an input file. The input file is most useful for collecting data at many points, as the process of entering all the data point information by hand can become tedious. The naming convention for the output is “filename.sel”. The following section addresses the use of the “output at selected locations” option.

### 7.7.2 Selected Output at Points/Lines/Rectangular Sub-regions

As stated above, there are two available methods for specifying output locations; by keyboard input and by reading from a file.

**Keyboard input.** Table 1 summarizes the information needed for the “keyboard input” option for extracting CGWAVE predictions at points, along lines and in rectangular sub-regions. Results may be obtained for more than one type of location in a given “trans” run.

Table 1. Summary of Input Information, Keyboard-Selected Output Option

Method of Specifying Location	Keyboard Input Information Needed by Program “trans”
Specific nodes	Total number of nodes, node numbers
(x,y) locations (points)	Total number of points, (x,y) coordinates
Lines (data collected along transects)	Total number of lines, (x,y) location of start point, (x,y) location of end point, number of intervals* between points.

Rectangular sub-regions	(x,y) location of corner points in clockwise order beginning from upper left point, number of intervals* between points 1 and 2 and between points 3 and 4.
-------------------------	---

\*Number of intervals between points may be specified as different values for each line.

Program “trans” will ask the user a “yes/no” question regarding each method of specifying the output location. A “no” answer skips to the next method. A “yes” answer will result in additional prompts for input information. After the input is complete, the program progresses to the next method.

**Input File Format.** The same output location data given in Table 1 is also used for the “input file” option. The input file format is given below. The naming convention for this file is “filename.pls”. The “%” symbols are comments and are not read by program “trans”, however, lines beginning with “%” should not split the individual data blocks. The meaning of each number is described in the data block. The sample file listed below includes all available output options, denoted by their flags “&id” for node Ids, “&pt” for (x,y) points, “&ln” for transects, “&rc” for rectangular sub-regions. The option blocks do not need to appear in the order shown, nor do all option blocks need to be present. For example, if the user wishes to specify data output from a single (x,y) location, then the input file need only contain the “&pt” flag on the first line, the quantity of points (1 in this example) on the second line, the x,y location of the point on the third line and the “end of data” statement on the last line. Note that the “end of data” statement must be the last line of the file.

```
% Top of File
%
% This file may be named *.pls, for point, line and square.
%
% This file provides information for selected output locations.
%
```

```

% Circular island problem
%
% Selected id flag
% Total number of node ids
% id numbers
&id
5
10 23 78 55 36
%
% Selected points flag
% Total number of points
% x y location of each point
&pt
3
-8972.0 -6884.0
3310.0 12353.0
463.0 14456.0
%
% Selected Lines flag
% Total number of lines
% x y of start point x y of end point
% number of intervals between points
&ln
3
10000.0 0.0 37000.0 0.0
29
0.0 10000.0 0.0 37000.0
29
-10000.0 0.0 -37000.0 0.0
29

```

```
%  
% Rectangular Sub-domain flag  
% upper left corner  
% upper right corner  
% lower left corner  
% lower right corner  
% number of intervals between first two corners  
% number of intervals between last two corners  
&rc  
-4.0 4.0  
4.0 4.0  
4.0 -10.0  
-4.0 -10.0  
9  
29  
end of data
```

## 7.8 Viewing Solutions in SMS

Any of the \*.sol files created by program “trans” contain wave information that can be read, viewed and printed by SMS. To do so, open SMS and then open the corresponding \*.geo file. The “Data Browser” tool (also found under the “Data” menu) is used to import the solution file. After opening the “Data Set Browser” window, select the “Import”. When the “Import Data Set” window appears, select “Generic file”. Choose the appropriate \*.sol file from the “Open” window. When viewing Amplitude/Phase solutions, three time step values will appear in the “Time” window (to the right of “Scalar data set”) in the data set browser. The time value “0.0” corresponds to wave amplitudes (which have values greater than or equal to 0.0). Time “0.5” corresponds to wave phases (values from -1.0 to 1.0). Time “1.0” corresponds to sea surface elevation (both positive and negative values). After choosing the type of solution to view, click the “Done” button. The solution contours, or vectors if vector data has been selected, will appear

within the modeled domain. Contours and vectors can be manipulated using the “Display Options” tool to provide a meaningful image.

## 7.9 Instructions for CGWAVE Interface in SMS (MODE-2 Usage)

### 7.9.1 Creating a Size Function

1. Import the .xyz data:

*File Menu:* choose *Import*

Select the *XYZ data* button.

Click *OK*.

Find and select an xyz data file (bp.xyz, for example), click *OPEN*.

2. In the *Mesh Module* follow these steps in sequence:

*Data Menu:* choose *Switch Current Model*.

Select *CGWAVE*.

Click *OK*.

*CGWAVE Menu:* choose *Create Functions*.

Leave only the *Wavelength* option on (turn all others off).

Enter desired value for period.

Click *OK*.

*Data Menu:* choose *Data Calculator*

Select *a. Wavelength* in text window (upper left).

Click *Add to Expression*.

Select “/” (divide symbol) in the calculator.

Enter desired number of elements in each wavelength (i.e.,10) as denominator.

Change the title “new data set” to “size” (i.e. name the newly created function).

Click on *Compute*.

Click *Done*.

## 7.9.2 Creating the Background Scatter Set

1. Create Scattered Data Set

*Data Menu: choose Mesh->Scattered Data*

Click *OK* – the name “scatter” is assigned to the set you just created.

2. Select Interpolation Method.

Switch to *Scatterpoint Module*.

*Interpolation Menu: choose Interp Opts.*

Choose *Inverse Distance Weighted*.

Click *Options*.

Choose *Constant (Shepherd's Method)*.

Click *OK* (Options Dialog).

Click *OK* (Interpolation Method Dialog).

## 7.9.3 Creating the Coastline and Inlet Arcs

1. Import the Coastline Arc.

Go to the *Map Module* and choose *Feature Objects/Coverages*.

Change the *Coverage* type on the bottom right of the dialog to *CGWAVE*.

Go to *File/Import* and choose the *Coastline* button.

Find the coastline file and push *OPEN*.

A brown *Coastline* type arc will be created.

2. Create the Inlet Arc.

Zoom in on the harbor area of the arc using the *Zoom* tool.

Use the *Create Feature Arc* tool to create an arc. The arc should be constructed such that it spans the harbor entrance and contains a single vertex located near the center of the harbor entrance (the arc will be made up of two end points and a vertex). Note: zoom on the Inlet part of the harbor and make sure that the end nodes of the new arc are placed exactly on one of the existing coastline arc vertices on the South and North sides of the inlet.

Using the *Select Feature Arc* tool, double click on the new arc.

Choose *Inlet* type when the arc attributes dialog. Press *OK* to exit the dialog.

Deselect the arc by clicking on a blank area of the screen (it is necessary to deselect any selected arcs before building polygons).

## 7.9.4 Defining Domains

### 1. Build Polygons and Define the Harbor Domain

In the *Feature Objects* menu, select *Build Polygons*.

Use the *Select Feature Polygons* tool to double click on the harbor area (which is a new polygon) and change the *CGWAVE* type to *Harbor*.

### 2. Defining the Domain from Coastline/Open Boundary Intersection Points.

Use the *Select Feature Vertex* tool to select a vertex on coastline corresponding to the point where the coastline and open boundary will meet. If no vertex exists at this location, an new vertex may be created using the *Create Vertex* tool.

With the vertex selected, go to *Feature Objects* menu: choose *Vertices <->Nodes*.

Repeat step 2 for the remaining coastline-open boundary intersection point.

Switch to *Select Feature Point /Node* tool.

Click the start point of the open boundary. Hold the SHFT key and click the end point of the open boundary. Keep in mind that the open boundary will be created in a counter-clockwise direction.

In the *Feature Objects* menu: choose *Define Domain*.

Enter the desired *Domain Type* and *OK* to exit.

### 3. Defining the Domain from the Harbor.

With the *Select Feature Vertex* tool, select the vertex in the middle of the Inlet (red) arc.

Go to *Feature Objects/Define Domain* and enter the desired values. Push *OK*. If a prompt appears saying that it was unable to create the domain, it will be necessary to change the settings in the *Define Domain* dialog.

### 7.9.5 Assigning Reflection Coefficients

Choose *Select Feature Vertex* tool.

Select vertices on the coastline where changes in the reflection coefficients are desired.

Go to *Feature Objects/Vertices<-> Nodes*. This splits the coastline arc. Each coastline arc can be assigned its own reflection coefficient. (Multiple vertices can be selected and converted to nodes at the same time by using the Shift key to multiply select the vertices).

Double click on each coastline arc and specify the desired reflection coefficient for that segment. (If more than one arc will have the same reflection coefficient, the arcs can be multiply selected using the Shift key and the attributes assigned using the *Feature Objects/Attributes* command.)

### 7.9.6 Assigning Open Ocean Attributes

Choose *Select Feature Arc* tool.

Select one or more open boundary arcs.

Select *Feature Objects/Attributes* command or double click on a single arc and specify the arcs as *Open Ocean* type. (Note: if a reflection coefficient is desired along an ocean boundary to simulate a near coastline type situation, the ocean boundary can be defined as a coastline. Use the instructions for assigning coastline reflection coefficients).

### 7.9.7 Setting the Active Scatter Data Function

Choose *Feature Objects/Build Polygons*.

Double click on the domain area to select the open ocean area of the domain and activate the attributes dialog.

Assign it to be an *Ocean* type.

Select the *Density* radio button and click on the *Options* button.

Select the “size” function (created in section 7.9.1) for Element Size and the “elevation” function for bathymetry.

Double click on the Harbor polygon and repeat *Density* operation.

### 7.9.8 Creating a Mesh from Feature Objects

De-select all polygons by clicking somewhere else on the screen.

Go to *Feature Objects/Map->2D Mesh* and push *OK* at the prompt.

Toggle the *Display Meshing Process* on if desired and push *OK*.

When meshing is completed, go to the *Scatter Module* and push *Display/Display Options* and toggle the scatter point symbols off for better viewing of the mesh (if desired).

### 7.9.9 Saving the CGWAVE .dat and .xyz (1-d) files

Go to the *Mesh Module*.

Click the *Select Nodestrings* button and select a nodestring (this is necessary for renumbering).

Choose *Elements/Renumber* and push *OK*. Push *OK* if prompted again.

Go to the *CGWAVE* menu, choose *Save Simulation*.

Select file names for the .dat and .xyz (1-d) files. If it is indicated that the 1-d file cannot be saved, go to *CGWAVE/Model Control* and increase the 1-d spacing or number of 1-d nodes.

### 7.9.10 Checking Mesh Quality

Go to *Scatter Module*.

Choose *Data/Data Browser* and select the size function used to generate the network.

Choose *Inerpolate/ ..to Mesh* and enter name of function for the new network to represent the target size for each element.

Go to *Mesh Module*.

Choose *CGWAVE/Create Functions* and turn off all functions except grid spacing.

Click *OK*.

Choose *Data/Data Calculator* and build size – grid function, call it “error”. This function should be close to zero. Areas with large values indicate node spacing that does not match the target spacing. If the spacing is too far off, contact BYU or edit mesh by hand. Another function useful for assessing mesh quality is the error/size, call it “pcnt\_err”. Areas with red color point to the elements, which are bigger than the target size, so refinement may be warranted.

### **7.9.11 Running CGWAVE**

CGWAVE can be run from *CGWAVE/Run CGWAVE*. Click on the file button to give the directory that contains the CGWAVE executable file.

# 8 EXAMPLES

Surface water waves have been modeled using CGWAVE for a number of idealized testcases and real practical applications. A number of these applications are presented here to both validate CGWAVE and to demonstrate its ability to model waves.

## 8.1 Shoal on a Sloping Beach

Surface water waves propagating over the shoal presented by Berkhoff, et al. (1982) were modeled. This test case demonstrates the ability of CGWAVE to simulate the effects of complex coastal bathymetric features. The shoal in Figure 7 is oriented such that the major axis of the shoal is parallel to contours of the water depth. Data is collected along the eight sections (transects) shown in Figure 7.

Normal incident, plane waves having a period of 1 second are modeled for all runs. An incident amplitude of 1.0 m is used for model runs using the linear dispersion relation. Runs that are made using the non-linear dispersion relation use an incident amplitude of 0.0232 m.

Results were compared for model runs made with different grid resolution. This was accomplished by varying the number of nodes in the computational domain and thus constructing different finite element grids. Nodes were located such that the number of nodes per wavelength remains constant throughout the domain. Grid densities from three to fifteen elements per (local) wavelength were used. The resulting finite element grids contain between 2500 and 75000 nodes and 5000 and 150000 elements, respectively. CPU time is not taken into account when comparing the quality of the model results, as the longest solution run is completed in less than four hours on a desktop (200 MHz processor) PC.

Figures 8, 9 and 10 show results for domains having resolutions of 3, 6, 8 and 15 nodes per wavelength. The numerical solution in Figure 8 shows little correlation to the lab data. The results in Figures 9 and 10 show a progression to the lab data as the resolution increases. The linear solution in Figure 10 matches the data better than either of the previous resolutions, however section 7 does not agree with the data in the region 6 to 10 meters behind the shoal. A grid resolution of about 10 or greater nodes per wavelength is generally thought to be necessary for an accurate solution to most problems.

The non-linear dispersion mechanism was applied only to grids containing 15 nodes per wavelength. This mechanism was not run for lower resolution grids because the linear amplitude solution is used in the formulation of the non-linear effect. Inclusion of the non-linear dispersion relation in the calculations has a noticeable effect on the solution for all sections (Figure 10). Sections 3 and 5 show a closer fit to the data in the areas to the left and right of center. Section 7 shows the most marked improvement in the region that begins 6 to 7 m behind the shoal.

This example problem showed that the results produced by the linear run of CGWAVE are good, provided that a fine enough grid resolution is used. The best results are obtained with the highest grid resolution. The addition of the non-linear dispersion relation (wave-wave interactions) mode shows a substantial improvement in the model estimates, yielding the best comparison to the measurements.

59-83.

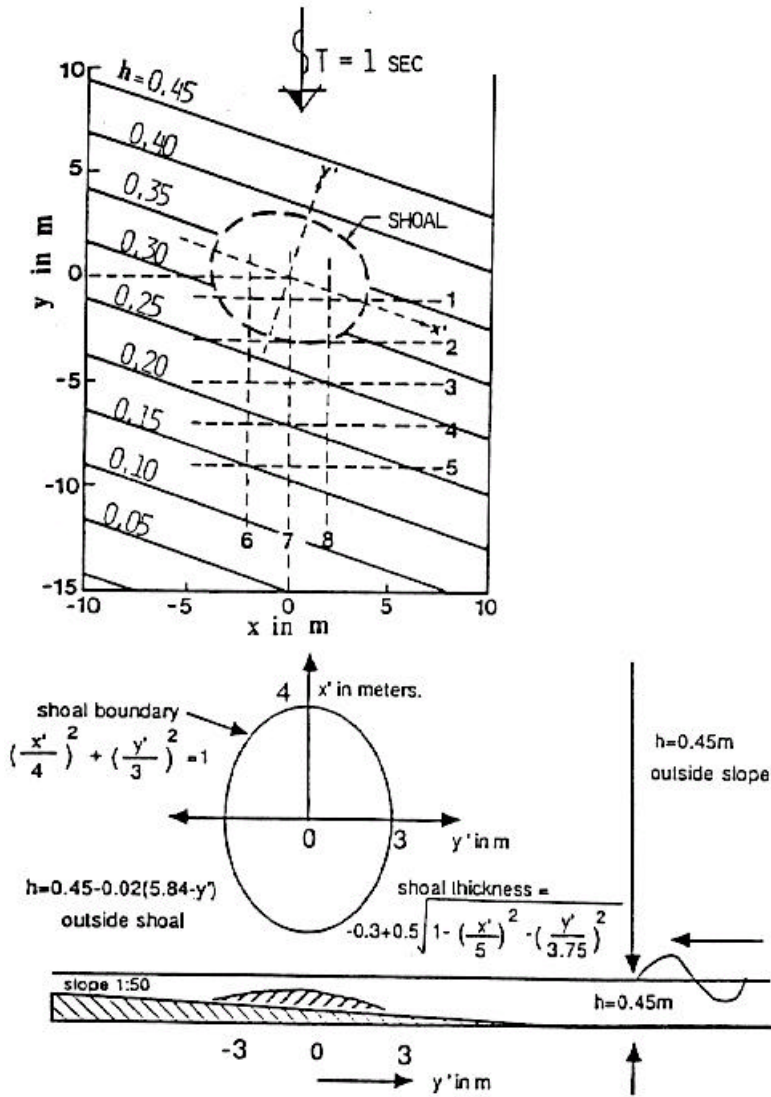


Figure 7. Modeled domain of Berkhoff et al. (1982)

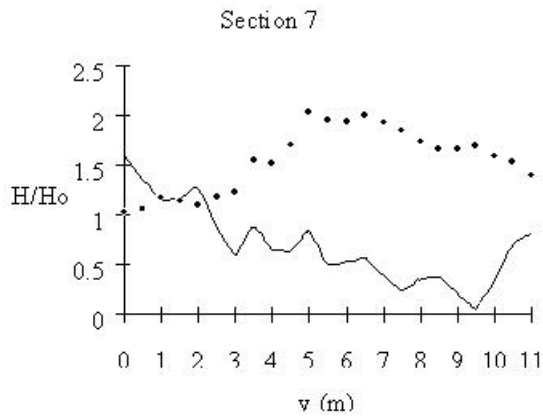
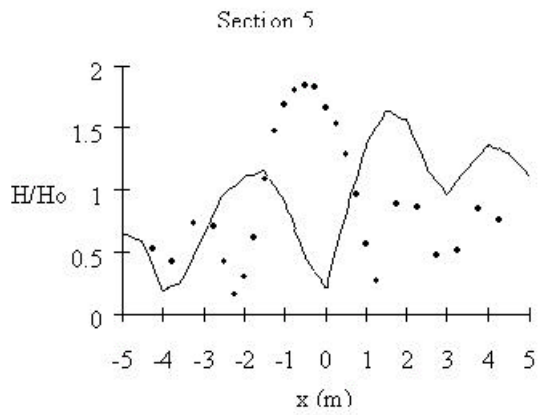
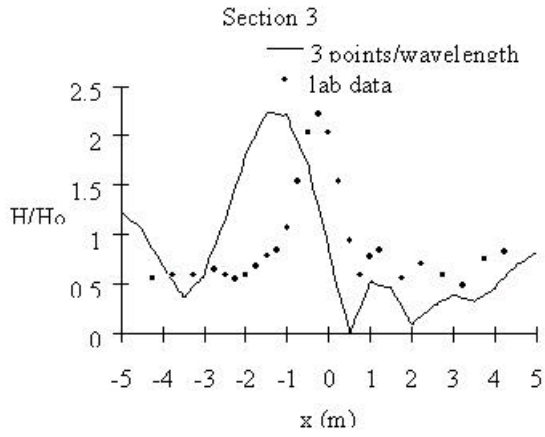


Figure 8. Wave height comparisons for a low resolution domain

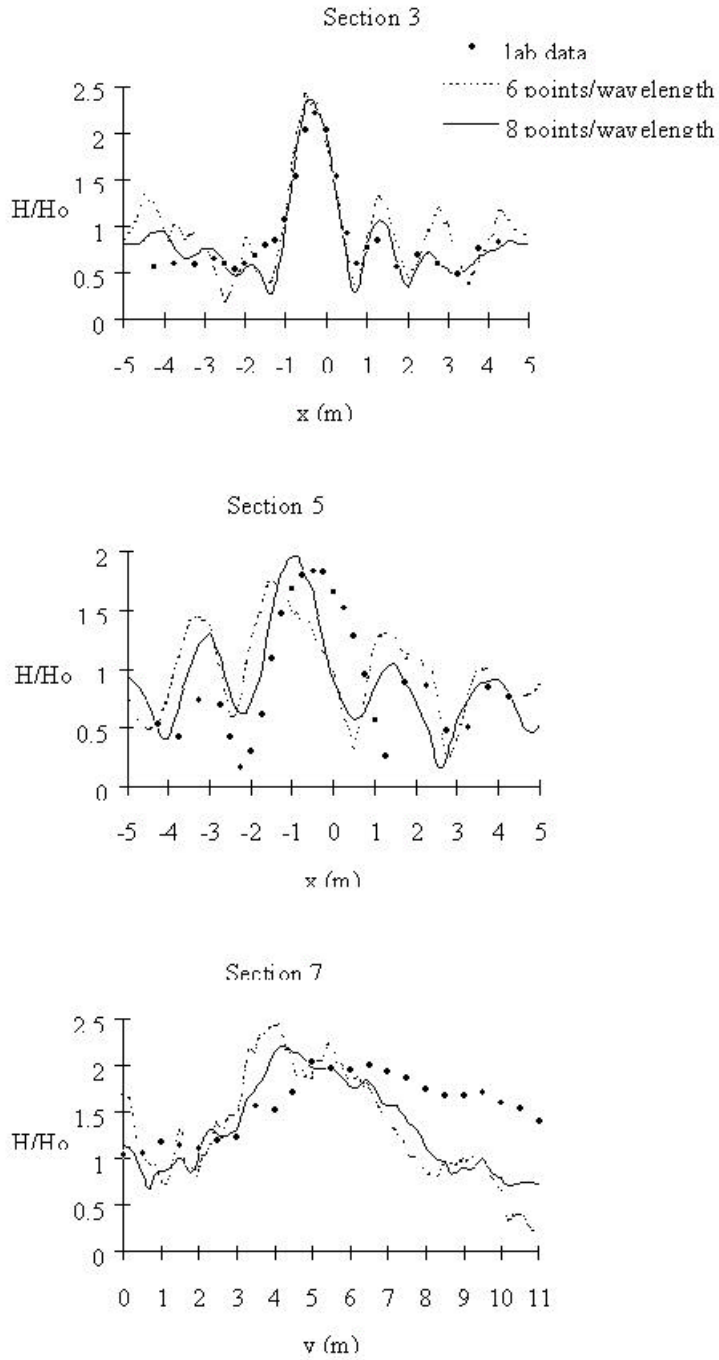


Figure 9. Wave height comparisons for increasing domain resolutions

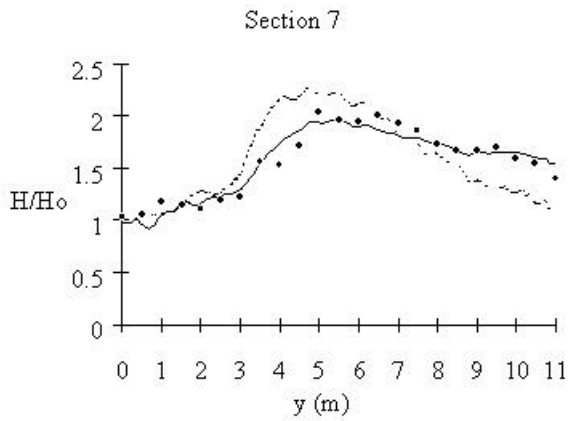
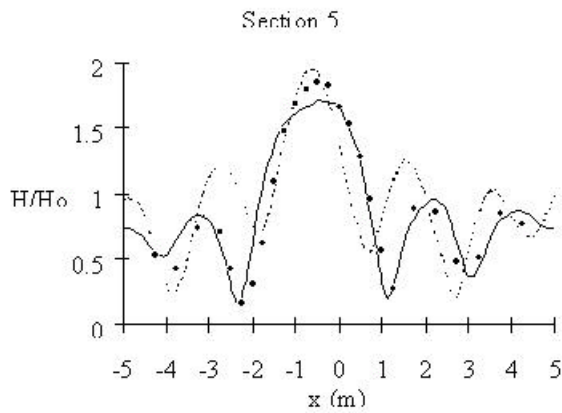
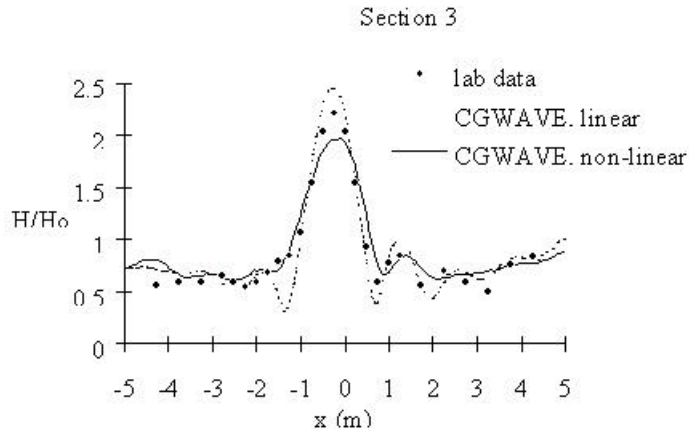


Figure 10. Wave height comparisons from linear and non-linear CGWAVE runs on a domain resolution of 15 points per wavelength

## 8.2 Irregular Wave Propagation Over a Shoal

The hydraulic model study of Vincent and Briggs (1989) was used to simulate spectral wave conditions in CGWAVE. The directional spectral wave generator (DSWG) at the Coastal Engineering Research Center of the U.S. Army Engineers was used to simulate refraction-diffraction of directionally spread irregular waves over an elliptic shoal. This study showed that spectral conditions can produce significantly different results than monochromatic waves. The model domain consists of an elliptic shoal surrounded by a region of constant depth. The orientation of the shoal and placement of coastal boundaries are shown in Figure 11. The minimum water depth over the shoal is approximately 0.15 m. The depth around the shoal is a constant 0.4572 m. Wave height data was collected along the nine sections indicated in Figure 11.

The spectral input to CGWAVE was constructed using a numerically generated, two-dimensional spectra,  $E(f,\theta) = E(f)D(\theta)$ . Expressions used for the energy spectrum,  $E(f)$ , and the directional spectrum,  $D(\theta)$ , follow. The energy spectrum is obtained using the Texel Marsen Arsloe (TMA) spectrum (Bouws et al. 1985, Panchang et al. 1990),

$$E(f) = g^2 \alpha (2P)^{-4} f^{-5} \exp \left\{ -1.25 \left( \frac{f_m}{f} \right)^4 + (\ln \gamma) \exp \left[ \frac{-(f - f_m)^2}{2\sigma^2 f_m^2} \right] \right\} \phi(f, h)$$

where  $\alpha$  = Phillips' constant

$f_m$  = peak frequency

$\gamma$  = peak enhancement factor (=1 for the Pierson-Moskowitz spectrum)

$\sigma$  = shape parameter ( $\sigma = \sigma_a$  if  $f < f_m$  and  $\sigma = \sigma_b$  if  $f \geq f_m$ )

$\phi(f,h)$  is a function that incorporates depth effects and is approximated by (Hughes 1984) as

$$\phi = \begin{cases} 0.5(\omega)^2 & \text{for } \omega_h < 1 \\ 1 - 0.5(2 - \omega_h)^2 & \text{for } 1 \leq \omega_h \leq 2 \\ 1.0 & \text{for } \omega_h > 2 \end{cases}$$

where  $\omega_h = 2\pi f(h/g)^{1/2}$ .

The directional spectrum is calculated as follows (Vincent and Briggs 1989),

$$D(\mathbf{q}) = \frac{1}{2\mathbf{p}} + \frac{1}{\mathbf{p}} \sum_{j=1}^j \exp\left[-\frac{(j\sigma_m)^2}{2}\right] \cos j(\mathbf{q} - \mathbf{q}_m)$$

where  $\theta_m =$  mean wave direction =  $0^\circ$

$j =$  number of terms in the series (20 in numerical calculations)

$\sigma_m =$  spreading parameter

The same functions  $E(f)$  and  $D(\theta)$  were also used in the laboratory study by Vincent and Briggs (1989) to construct a number of frequency and directional spectra (for details, see Vincent and Briggs 1989 or Panchang et al. 1990). One spectral case, B1, consisted of a broad frequency spectrum; the other case, N1, had a narrow frequency spectrum. The input data are summarized in Table 2. Two monochromatic and two spectral cases are shown. The incident wave height is  $2[2E(f)D(\theta)\Delta f\Delta\theta]^{1/2}$ .

Table 2. Model Input Data

Input	Case ID	Period (sec)	Significant Wave Height (m)	$\alpha$	$\gamma$	$\sigma_m$
Monochromatic	M1	1.3	.0550	--	--	--
	M2	1.3	.0254	--	--	--
Broad-directional	B1	1.3	.0775	.01440	2	$30^\circ$
Narrow-directional	N1	1.3	.0775	.01440	2	$10^\circ$

The discretization of the directional spectrum is summarized in Table 3. Other researchers have used the following discretizations. Panchang et al. (1990) used a directional bin width ( $\Delta\theta$ ) of  $4.39^\circ$  in a range from  $45^\circ$  to  $+45^\circ$ , resulting in 39 directional components for all spectra. Zhao and Anastasiou (1993) found that as many as 63 components were needed for the B1 and N1 cases. Li et al. (1993) produced results that suggest that an adequate solution can be obtained with as few as five directional components and five frequency components. In light of the results of Li et al. (1993), it

was decided that some exploration of the necessary number of directional components was in order.

Table 3. Directional Resolutions Used for Model Input

Case ID	Number of Directional Components (bins)	$\Delta\theta$ (°)
B1	9	20
	29	4.14
N1	5	12
	15	4

Tests were also performed to quantify the effects of the boundary conditions on the solution. It was hypothesized that reflections from the coastal boundaries (simulated walls of the wave tank) and improper treatment of these fully absorbing boundaries could cause significant variations in the final solution, especially for components with large angles of incidence. This hypothesis was tested by comparing the results obtained from two domains. Domain A closely approximated the physical model and contained coastal boundaries (Figure 11). Interior and exterior boundaries were considered fully absorbing ( $K_R = 0.0$  and  $K_{EXT} = 0.0$ ). Domain B used a full circle as an open boundary and contained all the depth variations (Figure 12). It was found that the boundary conditions do not significantly effect the results from CGWAVE in the area of interest. Results are only presented for Domain A.

CGWAVE results for the monochromatic conditions M1 and M2 are shown in Figures 13 and 14. The wave amplitudes double behind the shoal and decrease on the sides of the shoal. The linear model results show a similar pattern. The non-linear numerical calculations match the data better than the purely linear results. The data shows that the maximum wave height occurs further behind the shoal than predicted by both linear and non-linear solutions (section 7, Figures 13 and 14).

The CGWAVE results for the B1 spectral wave condition with  $\Delta\theta = 20^\circ$  discretization is shown in Figure 15. The result exhibits finger-like areas of large and

small wave height radiating away from the shoal in the down-wave direction that are not present in the lab data. The model results in Figure 15 do not show the same level of modulation as the lab results. The N1 solutions, although not shown, exhibit the same down wave characteristics as the B1 solutions.

The numerical solution approaches the lab data when the directional resolution is increased. Figures 16 and 17 show the results for the B1 and N1 spectra, respectively, using  $\Delta\theta$  equal to  $4.14^\circ$ . The widths of the directional spectra were limited to  $\pm 60^\circ$  for B1 and  $\pm 30^\circ$  for N1 spectra, since negligible amounts of energy are outside this range. The finger like patterns found in the cases with large  $\Delta\theta$  were not seen in these results. This finding agrees with the observations made by Zhao and Anastasiou (1993) and Panchang et al. (1990) regarding the width of directional bins needed in the input spectra.

The effect of amplitude-dependent non-linear dispersion was examined for the B1 and N1 cases. Zhao and Anastasiou (1993) show an improvement in the numerical solution. The CGWAVE results are essentially unchanged (Figures 16 and 17). This occurs because CGWAVE operates on each spectral component independently. Once a linear solution for a given component is found, these solution amplitudes are used in the non-linear dispersion relation and the new solution is found. The new amplitudes are again used in the non-linear mechanism. These iterations continue until a convergence criterion is reached. The final solution to the component is saved and the model is run for the next component. The incident wave heights associated with each spectral component are, at their largest, an order of magnitude smaller than the significant wave height. The wave heights used to compute non-linear effects are only a fraction of the significant wave height, causing the non-linear dispersion relation to have a negligible effect.

For this problem, CGWAVE produces linear results that closely match the data for the monochromatic waves propagating over the shoal. The inclusion of wave-wave interaction has improved the quality of this solution. CGWAVE also produces linear results that closely match the data for the irregular wave cases when adequate directional

resolution is provided in the input spectra. The solution algorithm used in the current version of the model does not completely allow non-linear effects to be accurately represented for the spectral wave modeling. Other solution algorithms should be evaluated in order to determine whether or not they may yield results that more closely match the lab data.

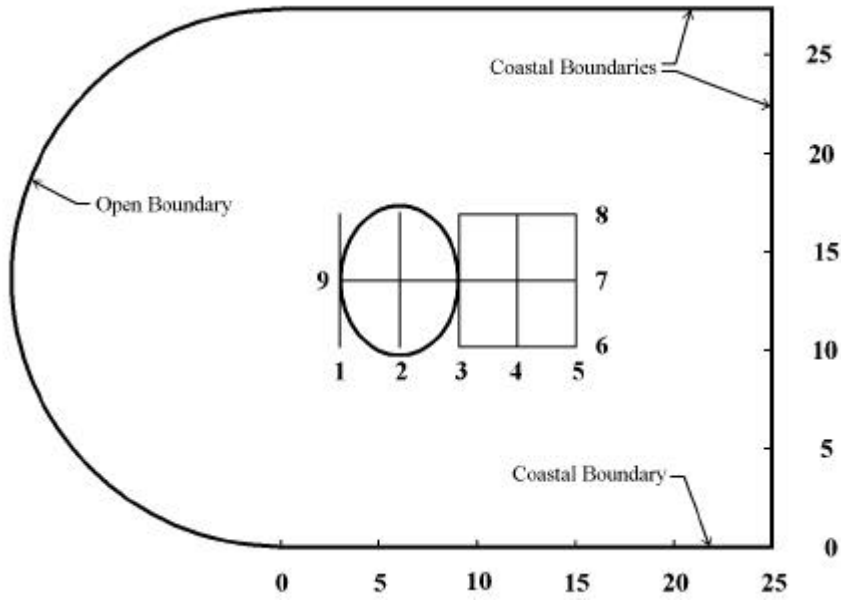


Figure 11. Model domain for wave propagation over an elliptic shoal [after Vincent and Briggs (1989)]

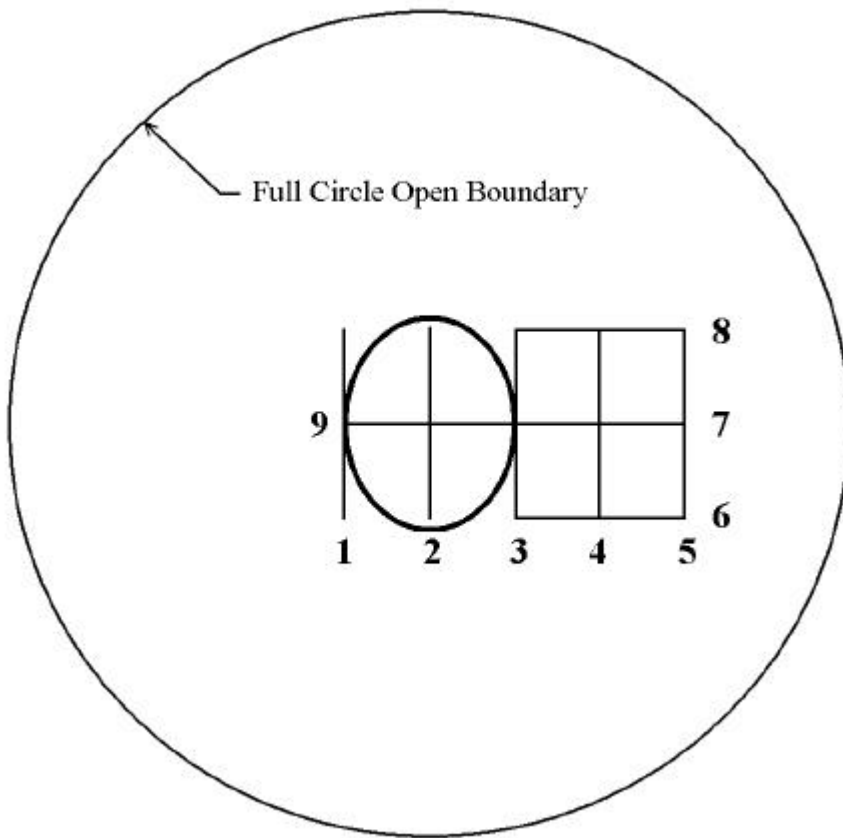


Figure 12. Domain without coastal boundary effects

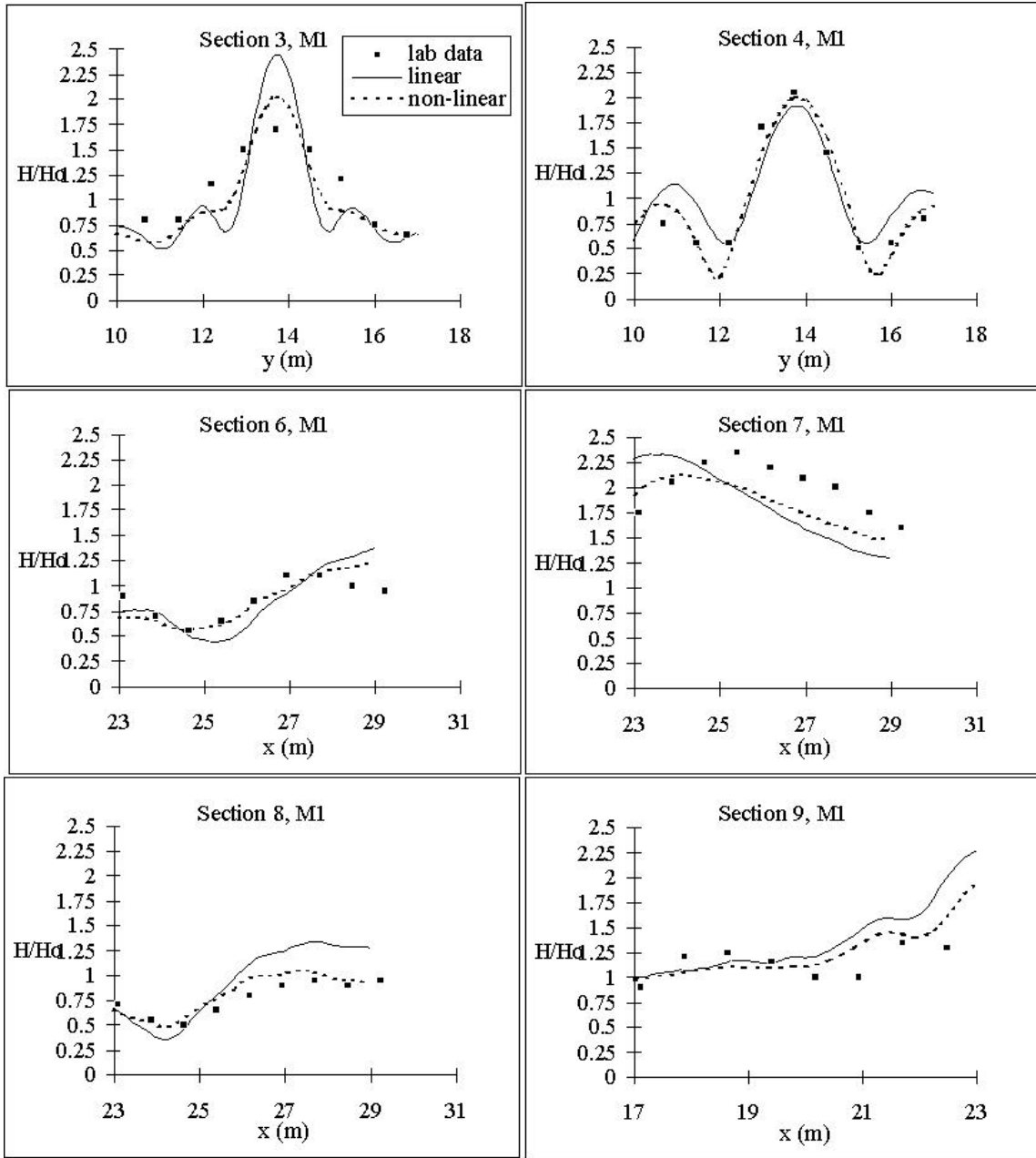


Figure 13. Wave height comparisons for M1 input condition

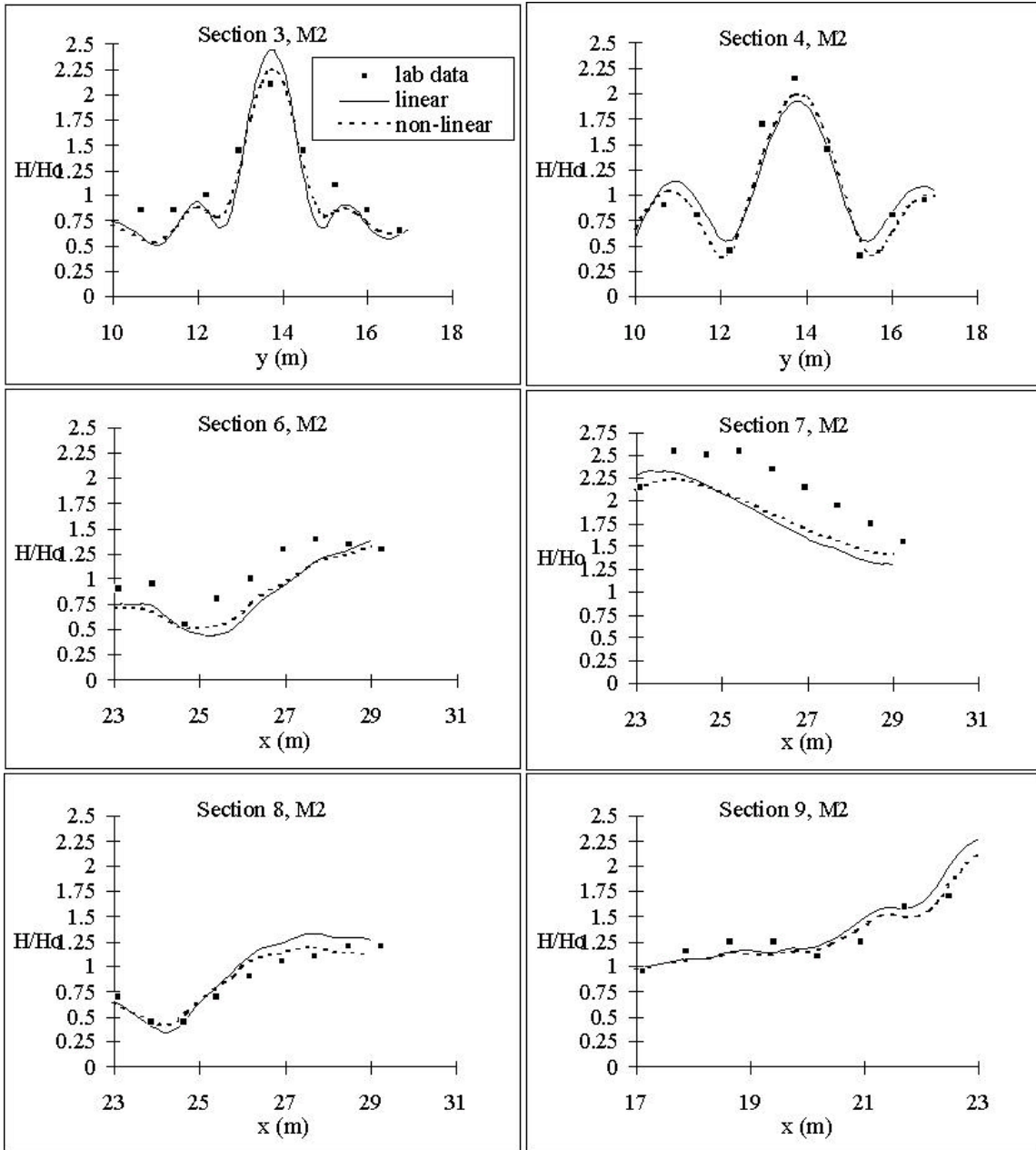


Figure 14. Wave height comparisons for M2 input condition

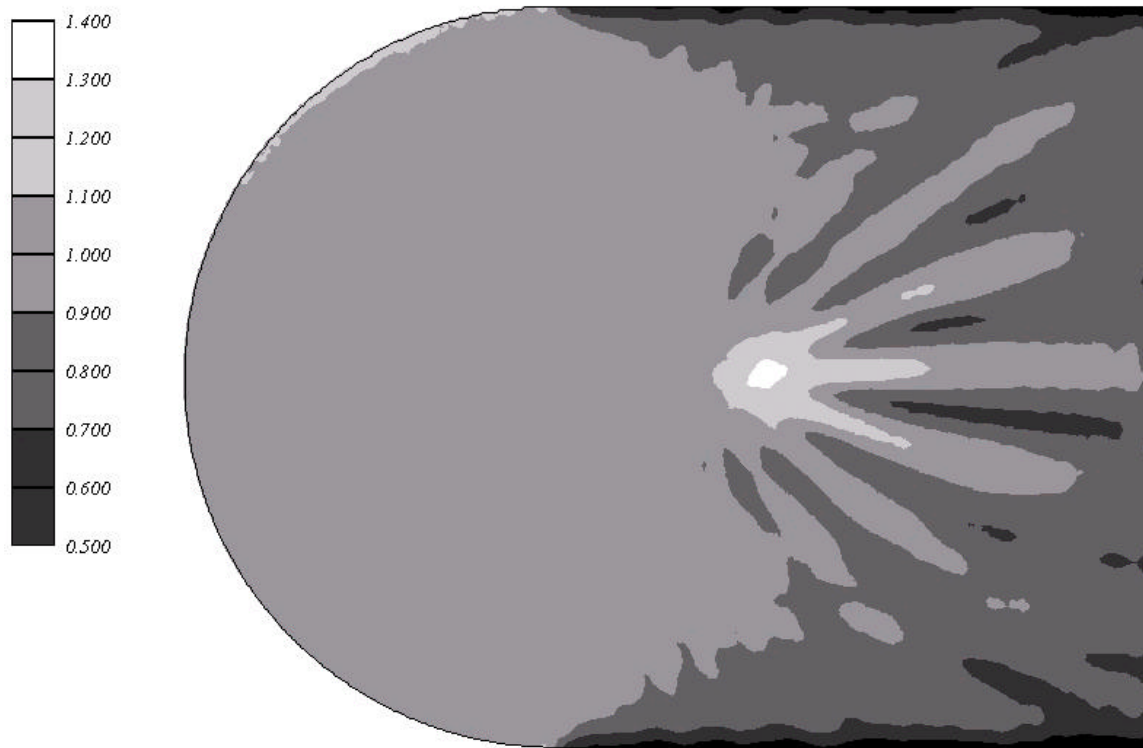


Figure 15. Estimated wave heights for B1 input spectrum, 20° directional discretization

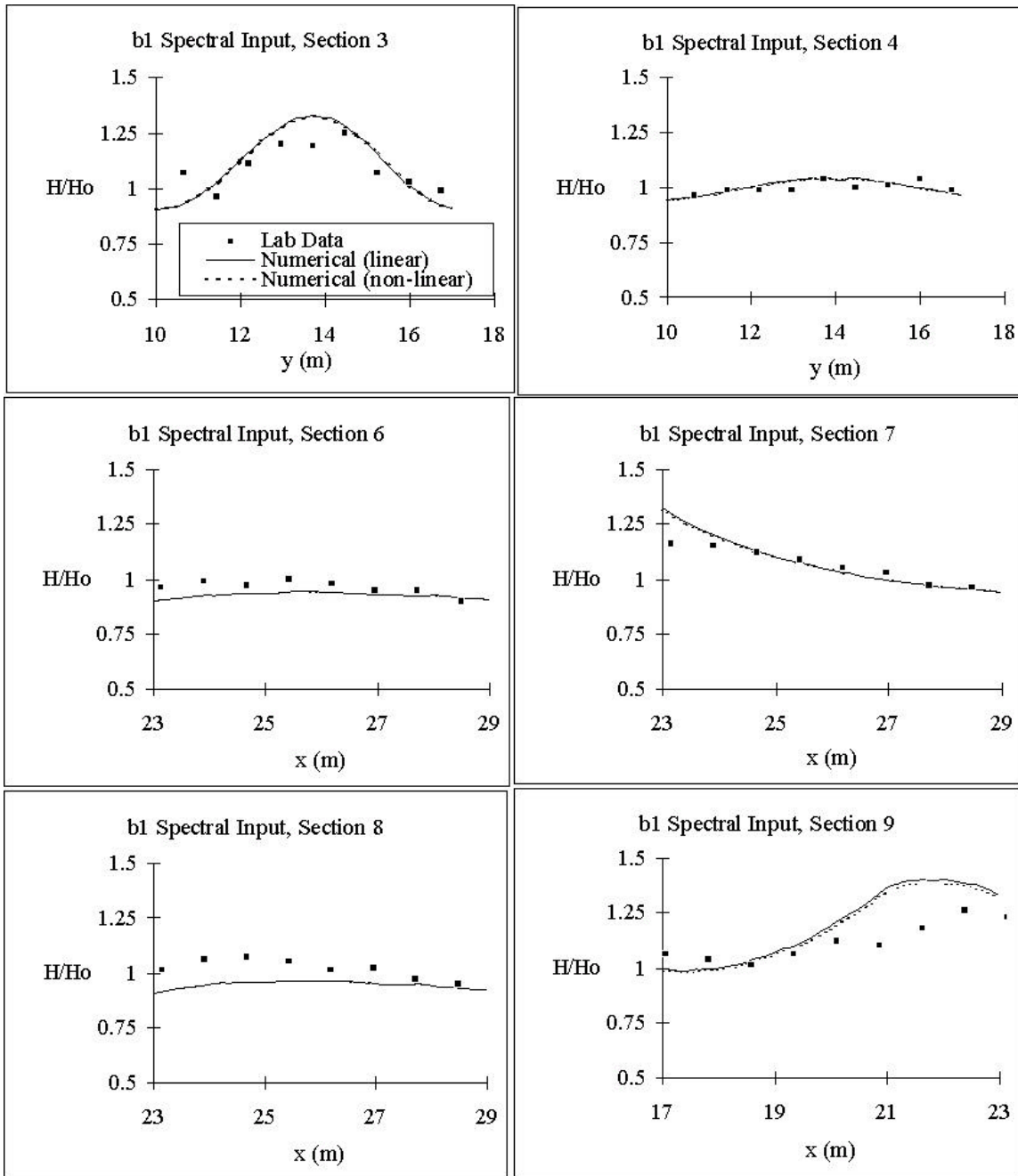


Figure 16. Wave height comparisons for B1 input condition,  $4.14^\circ$  directional discretization

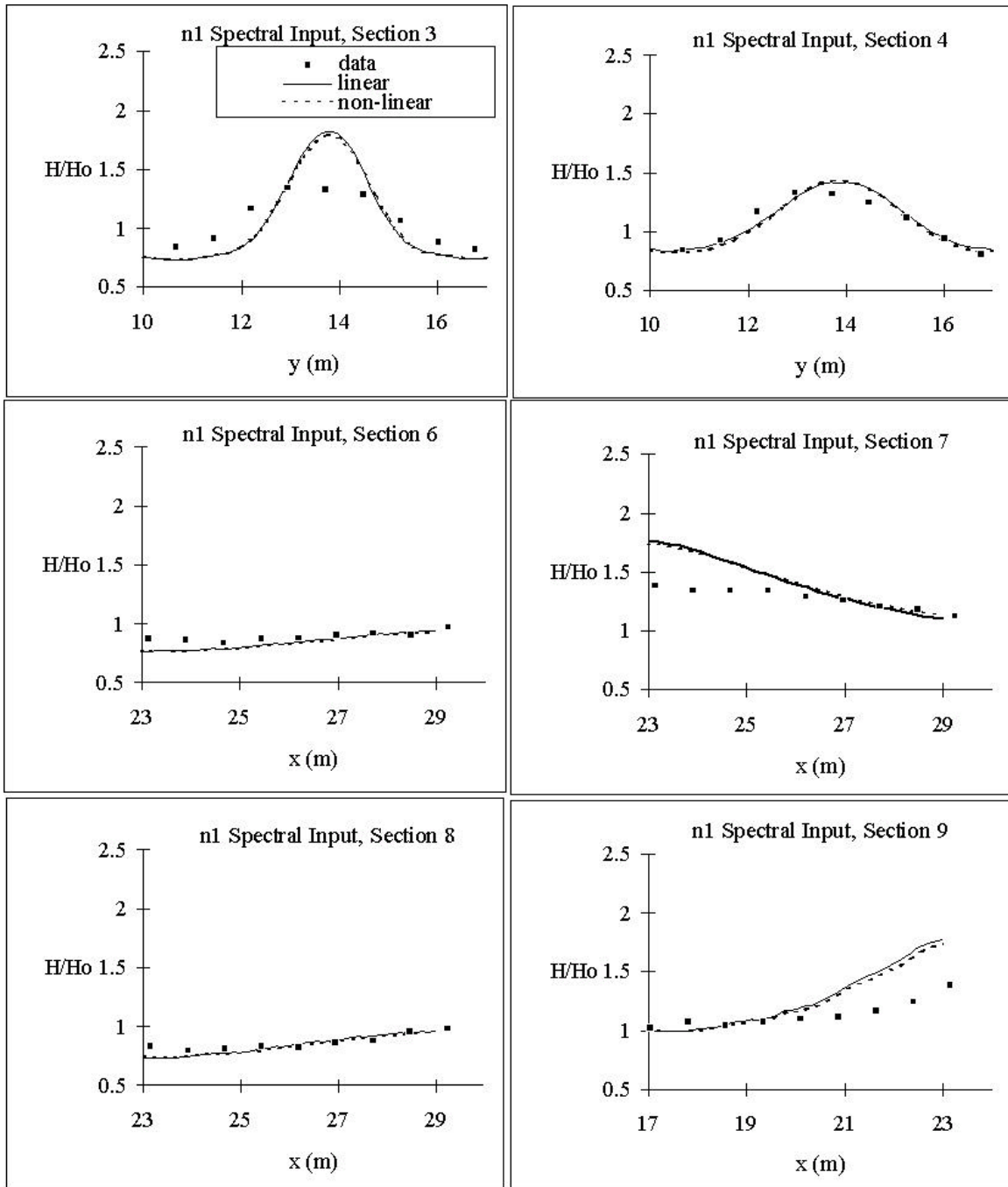


Figure 17. Wave height comparisons for N1 input condition,  $4.14^\circ$  directional discretization

### 8.3 Rectangular Harbor - Resonance

In this example, we examine the influence of bottom friction on dispersion of wave energy by friction for resonating waves in a rectangular harbor. The open boundary and harbor dimensions are shown in Figure 18. Theoretical and lab data for this case were presented in Ippen and Goda (1963), Lee (1971) and Chen (1986). Ippen and Goda (1963) showed that linear theory predicts amplitudes that are too large near the resonant frequency of the harbor. Chen (1986) examined the effects of bottom friction and coastal reflection on the amplitudes. Laboratory data was collected at the center of the back wall of the harbor (Lee, 1969).

Model input conditions were obtained from Lee (1969) and Chen (1986). Table 4 summarizes the input wave conditions.

Table 4. Model Input Data

Amplitude	$k/l$	Amplitude	$K/l$
.13	0.2	.30	1.8
.13	0.4	.25	2.0
.13	0.6	.25	2.5
.13	0.8	.30	3.0
.13	1.0	.25	3.5
.13	1.1	.35	4.0
.38	1.2	.35	4.2
.38	1.3	.35	4.4
.25	1.4	.25	4.6
.25	1.5	.30	4.8
.25	1.6	.30	5.0

The term  $k$  is the wave number and  $l$  (0.3111 m) is the length of the harbor. Variations in the friction coefficient and coastal reflection were considered. Waves were normally incident to the exterior boundary for all model runs.

Results for a fully reflecting harbor are shown in Figures 19, 20 and 21. The results of linear CGWAVE run without friction show a good match to the analytical solution of Ippen and Goda (1963) (Figure 19). Figure 20 shows that the amplification at

the resonant peaks decreases as the coastal boundary reflection coefficient decreases. These reflection coefficient does not affect the frequencies at which the resonant peak occurs.

Figure 21 shows the effects of friction on the CGWAVE predictions. As the friction parameter is increased, the solution shows a progression toward the lab data at the first resonant peak. The peak frequency shows a small shift for the larger values of the friction parameter. At the second resonant peak the solutions with friction match the solution without friction, indicating that energy dissipation due to bottom friction is less important for short period waves than for long period waves.

For this problem, CGWAVE reproduces laboratory data by including the effects of frictional dissipation and boundary absorption. The CGWAVE results show that harbor resonance is sensitive to the energy absorbed at the coastal boundaries and to dissipation by friction. The choice of friction parameter and coastal reflection coefficient does clearly affect the model estimates in resonance cases.

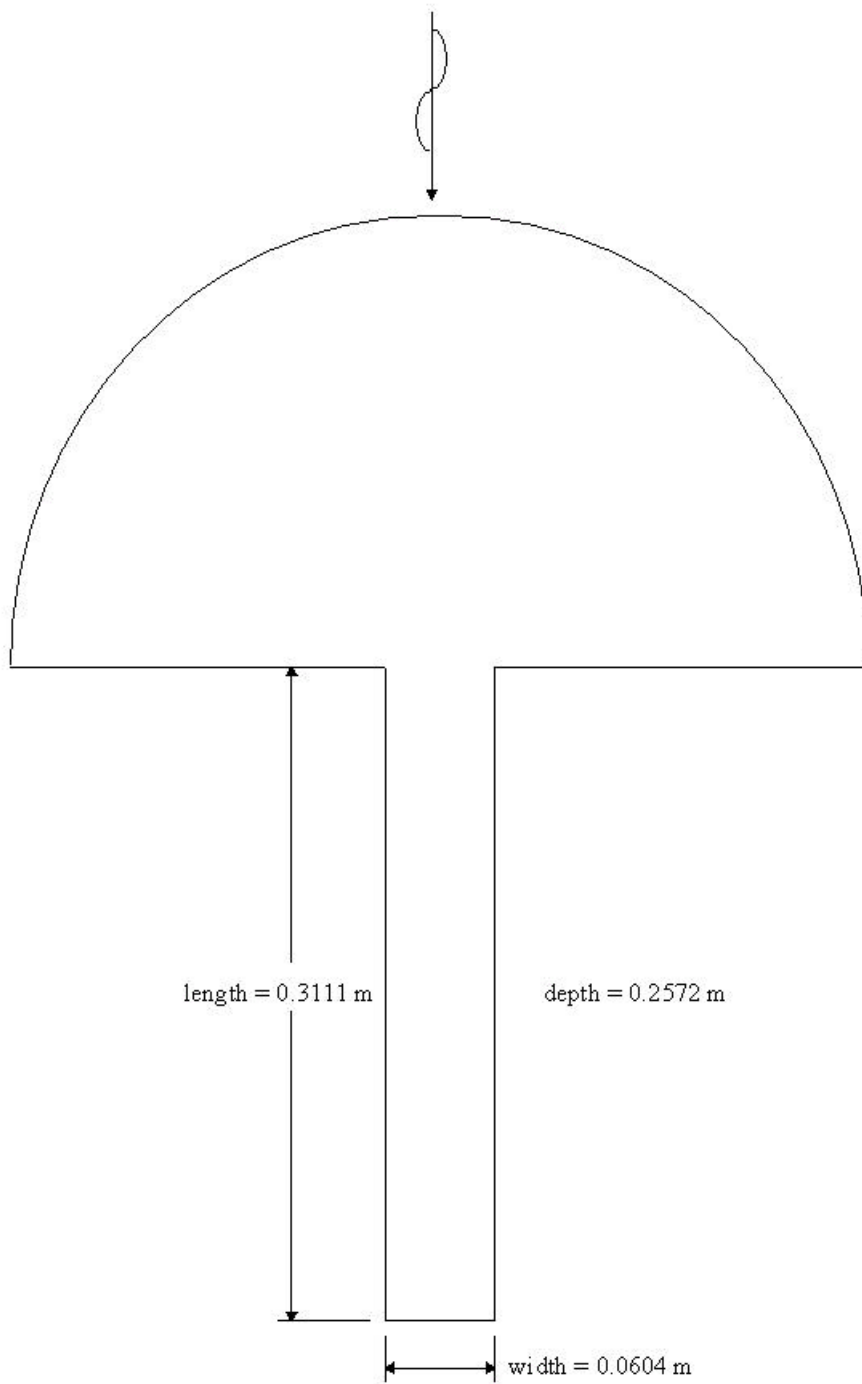


Figure 18. Rectangular resonance harbor with semi-circular open boundary

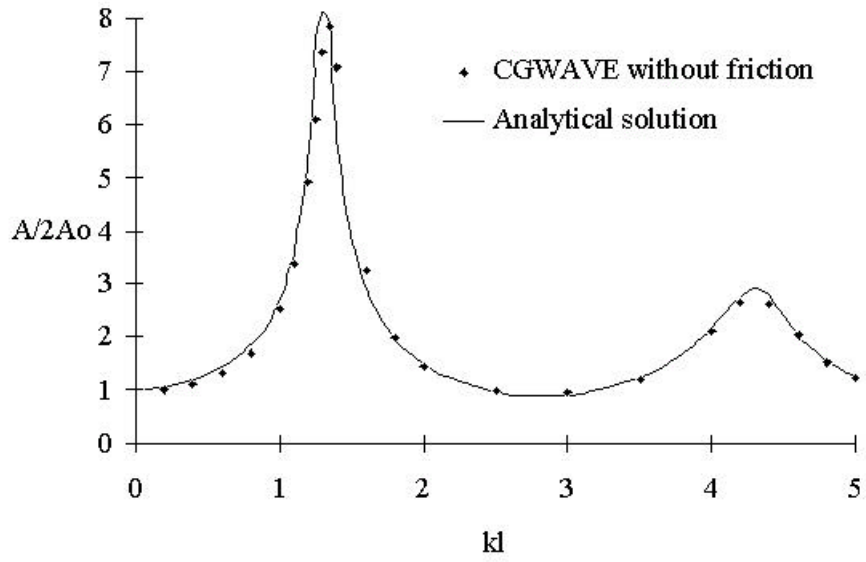


Figure 19. Theoretical and numerical resonance curves for a fully reflecting rectangular harbor

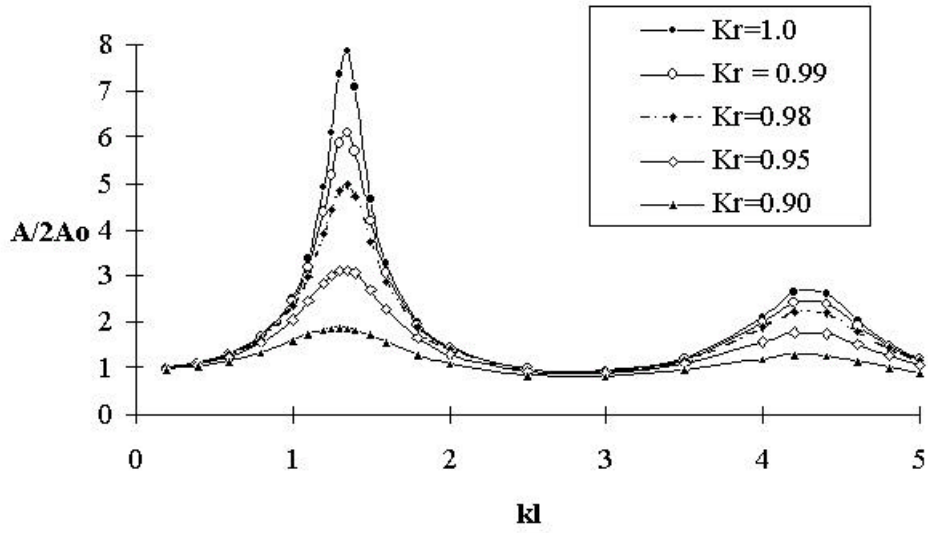


Figure 20. Harbor response curves for various values of coastal reflection coefficient

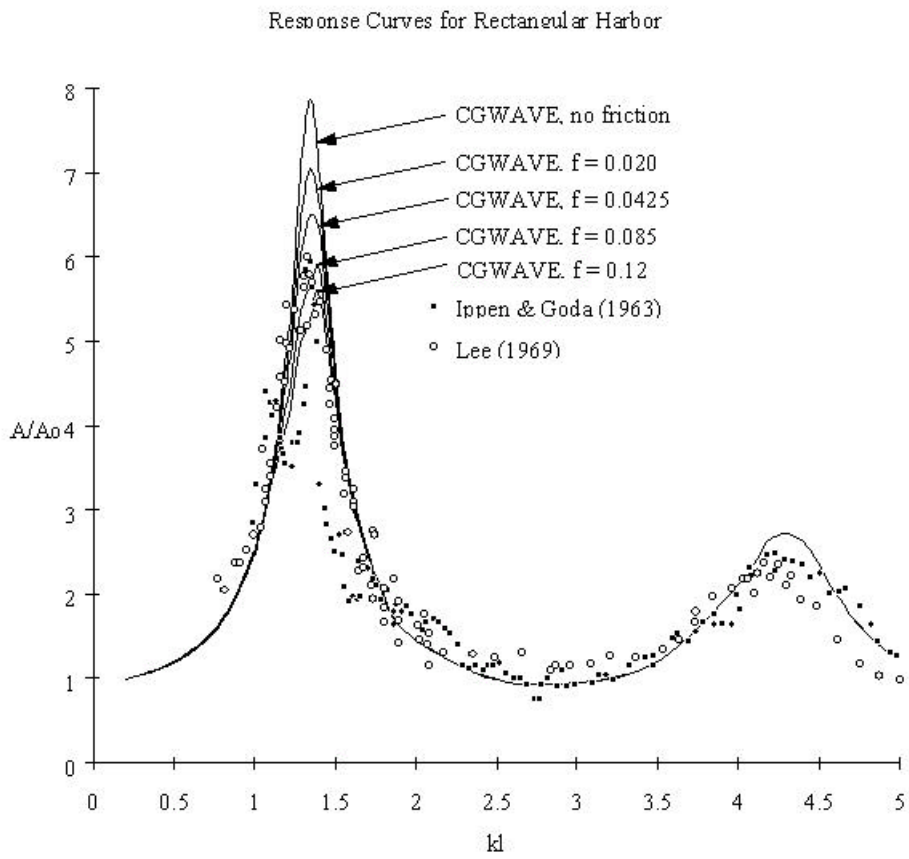


Figure 21. Harbor response curves for various values of the friction factor

## 8.4 Circular Island

In this example problem, we consider the propagation of long waves around a circular island is simulated. Homma (1950) and Jonsson, et al. (1976) showed that extensive scattering occurs for long waves. This case tests and demonstrates the ability of CGWAVE to handle strong scattering effects with a relaxed (Xu et al. 1996) boundary condition. This boundary condition allows the model to be applied to a greater range of modeling problems, as it does not require full reflection of the coastline outside the model domain.

The modeled domain (Figure 22) consists of a circular island on a shoal with a parabolic variation in depth. The island has a radius of 10 km. The open boundary is placed at a radius of 35 km from the center of the island. The minimum water depth is 444 m at the edge of the island and increases to 4000 m at the outer edge of the shoal. The domain has constant depth beyond the shoal. Incident wave periods of 240, 410 and 480 seconds are considered.

Figure 23 shows the results for the 240 second incident wave condition. This figure has been divided in half due to symmetry of the solution. Waves are incident from the left. The upper portion is the analytical solution, the lower portion is the CGWAVE result. The CGWAVE results match the analytical solution. Notably absent are signs of artificial boundary effects near the open boundary. Similar results were obtained for the longer wave periods, with results matching the analytical data.

Figure 22. Cross section of island and shoal bathymetry

Figure 23. Comparison of analytic and numerical wave amplitudes

## 8.5 Ponce de Leon Inlet, FL

This example shows the application of CGWAVE to Ponce de Leon Inlet, Florida. This inlet is the subject of a physical model study, allowing the comparison of laboratory data to CGWAVE model runs. Wave-current interaction may play a very important role on the wave fields to be predicted in coastal inlets (Demirbilek et al. 1996b); this capability will be available in CGWAVE model in the near future.

The coastline of the modeled domain is oriented in roughly a north/south manner. The modeled domain is bounded by a semi-circle of 2.5 km radius. A jetty extends into the domain from the north side of the inlet. The finite element mesh for this domain contains of about 118000 nodes and 234000 elements.

An example of a CGWAVE run of this domain is given. The wave phase diagram is shown in Figure 24 and estimated wave amplitudes are shown in Figure 25. The incident wave amplitude was 15 seconds. The incident wave direction was normal to the coastline. Coastlines were chosen to be fully energy absorbing (reflection coefficient of 0.0). Results from the numerical model are compared to laboratory data in Figure 26. The data comparison is made along a transect oriented parallel to the coastline and located several hundred meters to the south of the jetty. The CGWAVE model results for this case are shown prior to fine tuning of the numerical code and adjustment of model parameters. The study is in progress at the time of this writing. A detailed discussion of the results is expected to appear in a relevant scholarly journal at the conclusion of the study.

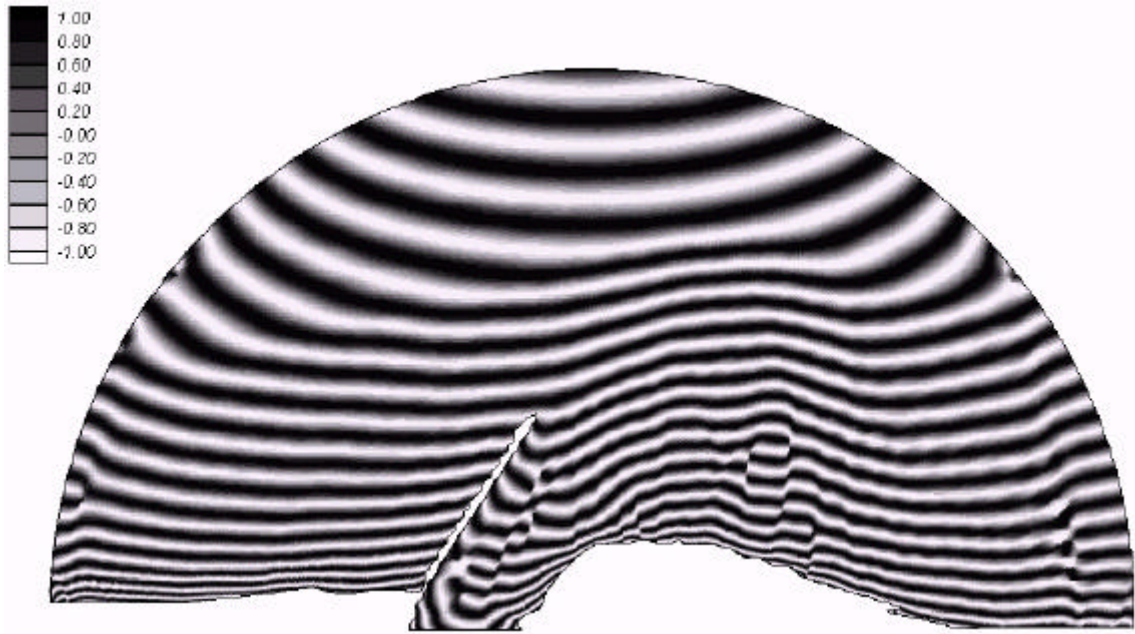


Figure 24. Phase diagram for normal incident direction, 15-second period wave condition



Figure 25. Estimated wave height diagram for normal incident direction, 15-second period wave condition

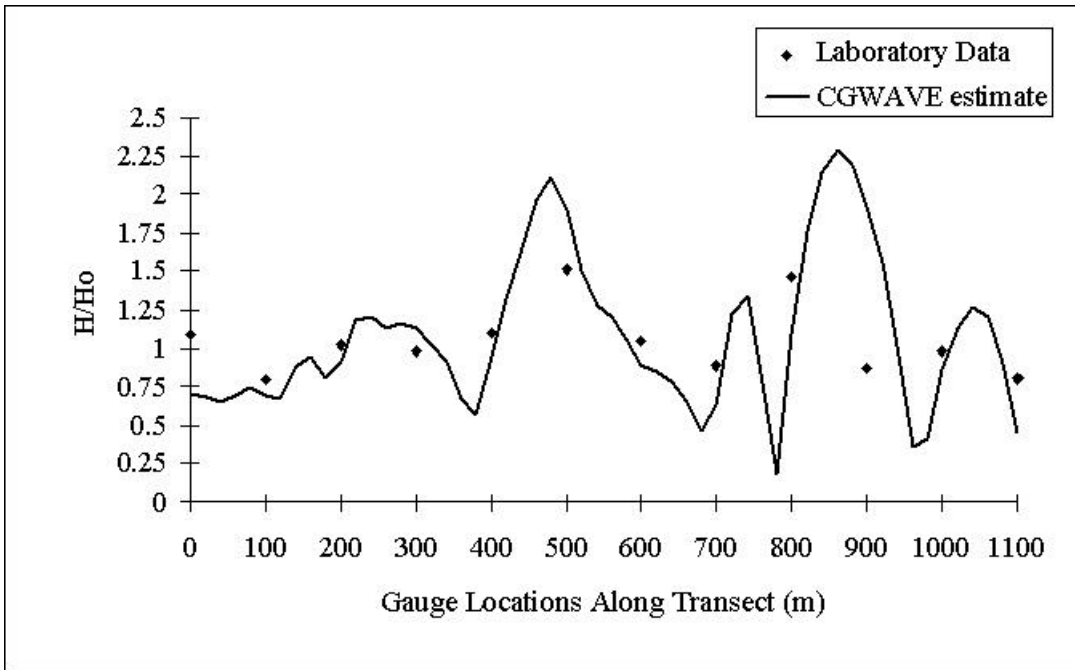


Figure 26. Comparison between laboratory data and CGWAVE wave height estimates along a transect

## 8.6 Barbers Point Harbor, HI

This example shows the application of CGWAVE to the harbor and near-by coastal regions of Barbers Point Harbor, Hawaii. A study is being conducted to explore harbor response to wave periods between 30 and 4000 seconds. Of particular interest are the contributions infragravity waves to the resonance of the harbor.

The modeled domain consists of the harbor area and a region outside the harbor of 3 km radius. The radius of the area outside the harbor is measured from the mouth of the harbor. This domain size allows multiple wavelengths to be modeled within the domain for all but the longest period waves. With appropriate resolution (based on the shortest period wave) the grid contains 33000 nodes and 65000 elements. Both monochromatic and spectral conditions are used as input in this modeling study.

An example of the estimated wave phases and amplitudes is given in Figures 27 and 28, respectively. These estimates are based on a normal incident input wave with a period of 100 s and incident amplitude of 1 m. The coastline has been assumed to be fully absorbing for this example case. A detailed analysis of the results of this study is in progress at the time of this writing. Comparisons of CGWAVE wave height estimates are to be made with field measurements in and around the harbor region. The results and analysis are to be documented in relevant journal articles upon completion of the study.

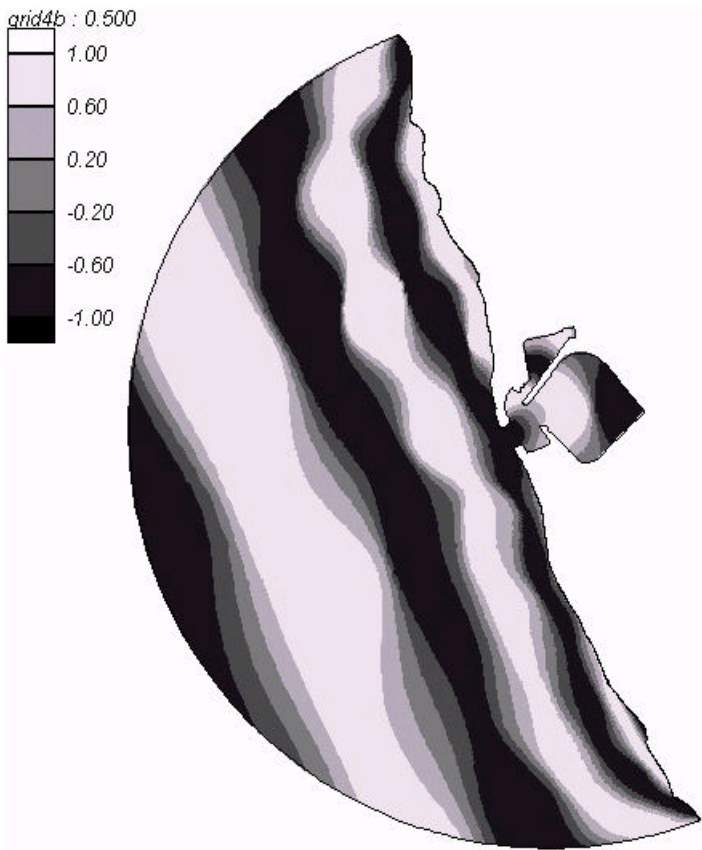


Figure 27. Wave phase diagram for normal incident direction, 100-second period wave condition

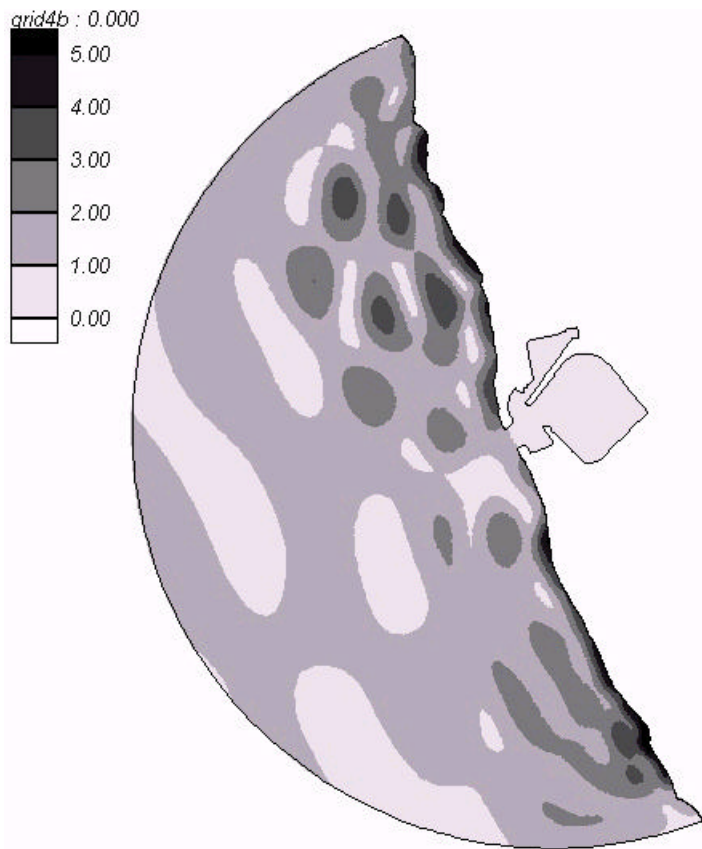


Figure 28. Estimated wave height diagram for normal incident direction, 100-second period wave condition

## 8.7 Onslow Bay, NC

This example shows the application of CGWAVE to New River Inlet in Onslow Bay, North Carolina. CGWAVE was applied to this region to provide wave height estimates for JLOTS (Joint Logistics Over-The-Shore) exercises.

A rectangular open boundary is used to separate the modeled domain from the open ocean. The modeled area outside the inlet is 3 km along shore by 2 km cross shore. The inlet area of the domain extends approximately 1.5 km inland. The finite element mesh for this domain contains of about 30000 nodes and 60000 elements. The grid resolution is good (no less than 10 nodes per wavelength) for waves of period equal to or longer than 35 seconds are.

The phase and amplitude results for a monochromatic wave simulation are shown in Figures 29 and 30, respectively. For this model run, incident waves were normal to the coastline. The incident wave period was 35 seconds. The incident wave height was 1 m. The coastline was assigned a reflection coefficient of 0.4. The alternating pattern of wave phase is shown in Figure 29. Wave heights of 2 m were predicted to the north side of the inlet, represented by the darkest color shown in Figure 30.

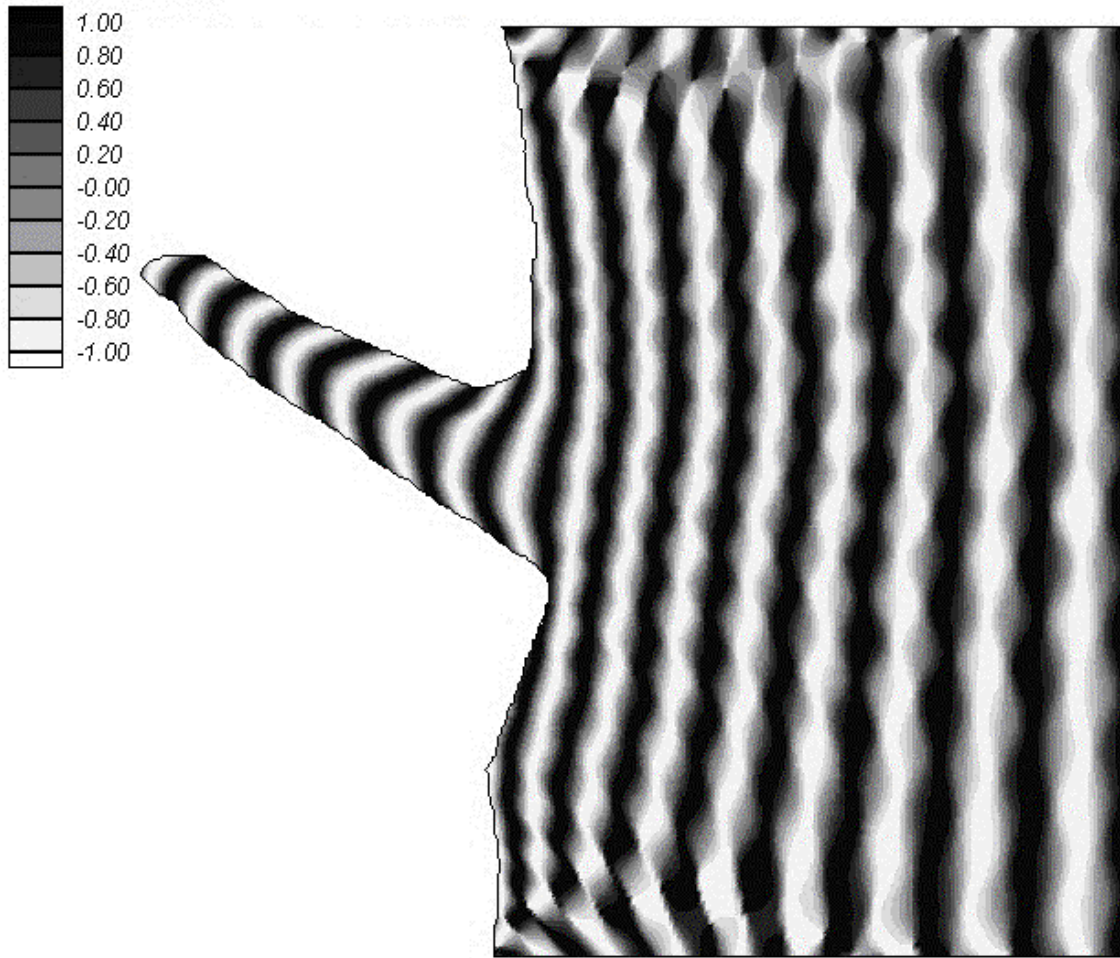


Figure 29. Wave phase diagram for normal incident direction, 35-second period wave condition

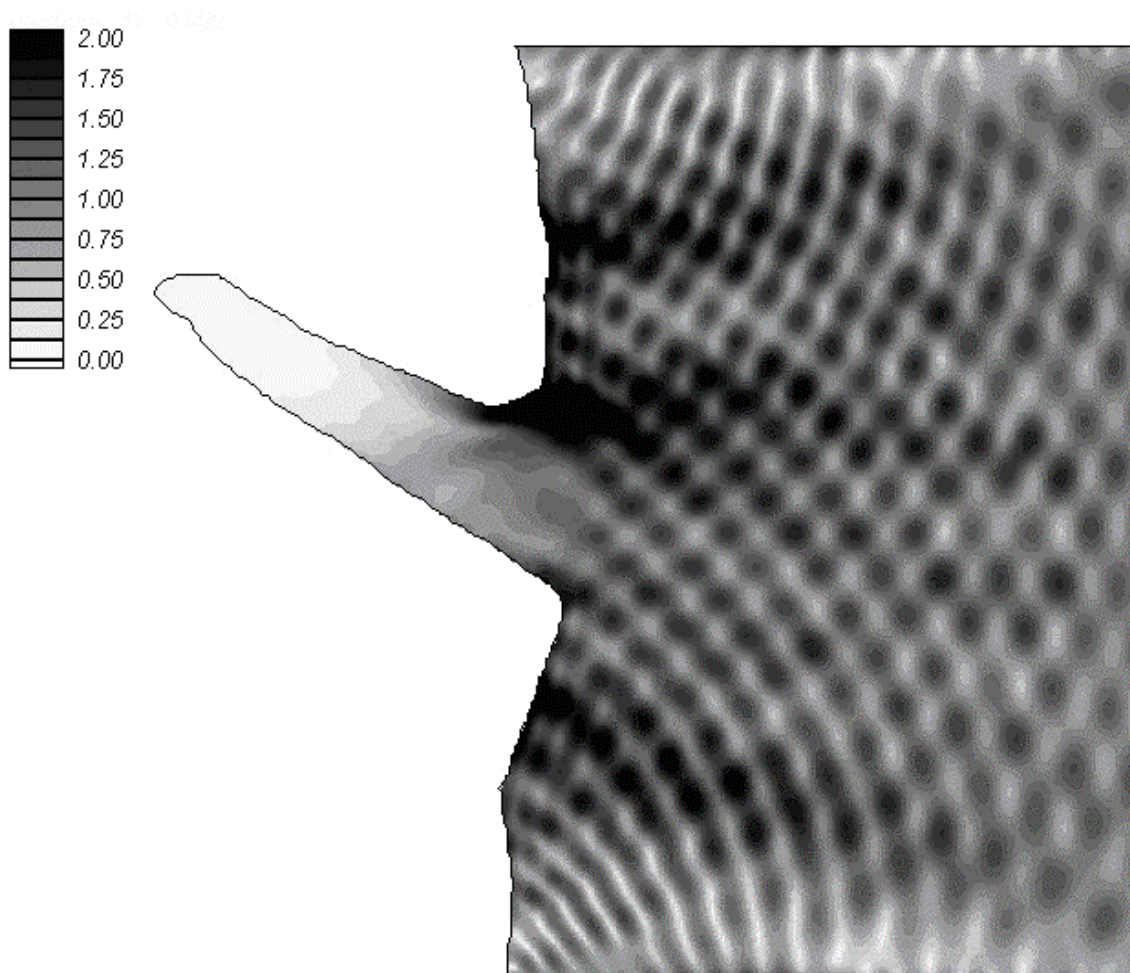


Figure 30. Estimated wave height diagram for normal incident direction, 35-second period wave condition

# References

- Berkhoff, J. C. W., Booij, N., and Radder, R. C. (1982). Verification of Numerical Wave Propagation models for Simple Harmonic Linear Waves, *Coastal Engineering*, **6**, 255-279.
- Berkhoff, J. C. W. (1976). Mathematical Models for Simple Harmonic Linear Water Waves Wave Refraction and Diffraction, *Publ. 163*, Delft Hydraulics Laboratory.
- Berkhoff, J. C. W. (1972). Computation of Combined Refraction – Diffraction, *Proc. 13<sup>th</sup> International Coastal Engineering Conference*, 741-790.
- Bouws, E., Gunther, H., Rosenthal, W., and Vincent, C. (1985). Similarity of the Wind Wave Spectrum in Finite Depth Water, Part I - Spectral Form, *J. Geophys. Res.*, **90**, 975-986.
- Chen, H. S. (1986). Effects of Bottom Friction & Boundary Absorption on Water Wave Scattering, *Applied Ocean Research*, **8**, 99-104.
- Chen, H. S. (1990). Infinite Elements for Water Wave Radiation and Scattering. *International J. Numerical Methods in Fluids*, **11**, 555-569.
- Chen, H. S. and J. R. Houston (1987). Calculation of Water Level Oscillations in Harbors, *Instructional Rept. CERC-87-2*, Waterways Expt. Stn., Vicksburg, Mississippi.
- Dally, W. R., R. G. Dean & R. A. Dalrymple (1985). Wave Height Variation across beaches of arbitrary profile, *J. Geophys. Research*, **90**, 1917-1927.
- Dalrymple, R. A., Kirby, J. T., and Hwang, P. A. (1984). Wave Diffraction due to areas of high energy dissipation, *J. Waterway, Port, Coastal and Ocean Eng.*, **110**, 67-79.
- Demirbilek, Z., (1994). Comparison Between REFDIFS and CERC Shoal Laboratory Study, *Unpublished Report*, Waterways Exp. Station, Vicksburg, MS, p 53.
- Demirbilek, Z. and Gaston, J. D., (1985). Nonlinear Wave Loads on a Vertical Cylinder, *Ocean Eng.*, **12**, 375-385.
- Demirbilek, Z. and Webster, W. C., (1992). Application of the Green-Naghdi Theory of Fluid Sheets to Shallow-water Wave Problems, Report 1: Model Development, Report 2: User's Manual and Examples for GNWAVE, U.S. Army Waterways Exp. Station, *Tech. Reports CERC-92-1 and CERC-92-13*, Vicksburg, MS.
- Demirbilek, Z. and Webster, W. C., (1998). A Shallow-water Wave Theory Based on Green-Naghdi Formulation, *Handbook of Coastal Engr.*, Vol.4 (ed. Herbich, J.B.), Gulf Publ. Co. (to appear).

Demirbilek, Z., Xu, B. and Panchang, V. (1996a). Uncertainties in the Validation of Harbor Wave Models, *Proc. 25<sup>th</sup> Intl. Coastal Engr. Conf.*, 1256-1267.

Demirbilek, Z., Briggs, M. and Green, D. (1996b). Wave-current Interaction at Inlets, *Proc. 25<sup>th</sup> Intl. Coastal Engr., Conf.*, 1219-1232.

De Girolamo, P., J. K. Kostense & M. W. Dingemans 1988. Inclusion of Wave Breaking in a Mild-Slope Model, *Computer Modeling in Ocean Engineering* (eds. Schrefler and Zienkiewicz), Balkema, Rotterdam, 221-229.

Ebersole, B.A. (1985) Refraction-Diffraction Model for Linear Water Waves, *J. Waterway, Port, Coastal and Ocean Eng.*, **111**, No. 6.

Homma, S. (1950). On the Behaviour of seismic Sea Waves Around a Circular Island, *Geophys. Mag.*, **21**, 199-208.

Ippen, A. T., and Goda, Y. (1963). Wave Induced Oscillations in Harbors: The Solution for a Rectangular Harbor Connected to the Open-Sea, *Hydrodynamic Laboratory Report No. 59*, Massachusetts Institute of Technology.

Jones N. L. and D. R. Richards (1992). Mesh Generation for Estuarine Flow Models, *J. Waterway, Port, Coastal and Ocean Engineering*, **118**, 599-614.

Jonsson, I. G., Skovgaard, O., and Brink-Kjaer, O. (1976). Diffraction and Refraction Calculations for Waves Incident on an Island, *J. Marine Research*, **343**, 469-496.

Kirby, J. T. (1986). Higher Order Approximation in the Parabolic Equation Method for Water Waves, *J. Geophys. Research*, **91**, 933-952.

14. Kirby, J. T. (1989). A Note on Parabolic Radiation Boundary Conditions for Elliptic Wave Calculations, *Coastal Engg.*, **13**, 211-218.

Kirby, J. T. & R. A. Dalrymple, 1984. Verification of a Parabolic Equation for Propagation of Weakly-Nonlinear Waves, *Coastal Engineering*, **8**, 219-232.

Kirby, J. T. & R. A. Dalrymple, 1986. An Approximate Model for Nonlinear Dispersion in Monochromatic Wave Propagation Models, *Coastal Engineering*, **9**, 545-561.

Kostense, J. K., K. L. Meijer, M. W. Dingemans, A. E. Mynett, and P. van den Bosch (1986). Wave Energy Dissipation in Arbitrarily Shaped Harbours of Variable Depth, *Proc. 20th Intl. Conf. Coastal Engineering*, 2002-2016.

Lee, J-J., 1971: Wave - Induced Oscillations in Harbors of Arbitrary Geometry, *J. Fluid Mech.*, **45**, 375-394.

Lee, J.J., (1969), Wave Induced Oscillations in Harbors of Arbitrary Shape, *Report No. KH-20*, W.M. Keck Laboratory, California Institute of Technology, Pasadena, p.266.

Li, B., (1994). A Generalized Conjugate Gradient Model for the Mild Slope Equation, *Coastal Engineering*, **23**, 215-225.

Li, B., Reeve, D.E., Fleming, C.A., (1993). Numerical Solution of the Elliptic Mild-Slope Equation for Irregular Wave Propagation, *Coastal Engr.*, **20**, 85-100.

18. Lie, V. and Torum, A. (1991). Ocean Waves over Shoals, *Coastal Engr.*, **15**, 545-562.

Liu, P.L.-F, 1983. Wave-Current Interactions on a Slowly Varying Topography, *J. Geophys. Research*, **88**, 4421-4426.

Liu, P. L.-F. and Tsay, T. K., (1984). Refraction-Diffraction Model for Weakly Nonlinear Water Waves, *J. Fluid Mech.*, **141**, 265-274.

Liu, P. L.-F. and Tsay, T.-K. (1985). Numerical Prediction of Wave Transformation. *J. Waterway, Port, Coastal and Ocean Eng.*, **111**, 843-855.

Madsen, O.S. (1976). Wave Climate of the Continental Margin: Elements of its Mathematical Description, *Marine Sediment Transport and Environmental Management* (eds. D. Stanley and D.J.P. Swift), John Wiley, New York, 65-87.

Mei, C. C. (1983). *The Applied Dynamics of Ocean Surface Waves*, John Wiley, New York.

Panchang, V. G., B. Cushman-Roisin, & B. R. Pearce (1988). Combined Refraction-Diffraction of Short Waves for Large Coastal Regions, *Coastal Engineering*, **12**,133-156.

Panchang, V. G., W. Ge, B. R. Pearce, & M. J. Briggs (1990). Numerical Simulation of Irregular Wave Propagation over a Shoal, *J. Waterway, Port, Coastal and Ocean Engineering*, **116**, 324-340.

Panchang, V. G., W. Ge, B. Cushman-Roisin, & B. R. Pearce (1991). Solution to the Mild-Slope Wave Problem by Iteration, *Applied Ocean Research*, **13**, 187-199.

Panchang, V. G. , B. Xu, & Z. Demirbilek (1996). Wave Models for Coastal Applications, *Handbook of Coastal Engineering*, Vol. 4 (to appear).

Panchang, V. G. and B. Xu, 1995. CGWAVE: A Coastal Wave Transformation Model for Arbitrary Domains, Tech. Report, Dept. of Civil and Environmental Engineering, University of Maine, Oct. 1995.

Tsay, T.-K., and P. L.-F. Liu, 1983. A Finite Element Model for Wave Refraction and Diffraction, *Applied Ocean Research*, **5**, 30-37.

Vincent, C. L. and Briggs, M. J. (1989). Refraction-Diffraction of Irregular Waves over a Mound, *J. Waterway, Port, Coastal and Ocean Eng.*, **115**, 269-284.

Xu, B. & V. G. Panchang (1993). Outgoing Boundary Conditions for Elliptic Water Wave Models. Proceedings, *The Royal Society of London, Series A*, **441**, 575-588.

Xu, B., V. G. Panchang and Z. Demirbilek, (1996). Exterior Reflections in Elliptic Harbor Wave Models, *J. Waterway, Port, Coastal, and Ocean Engr.*, **122**, 118-126.

Zhao, Y., and Anastasiou, K. (1993). Economical Random Wave Propagation Modelling Taking into Account Non-Linear Amplitude Dispersion, *Coastal Engineering*, **20**, 59-83.